

CO₂ / Sn LPP EUV Sources for device development and HVM

David C. Brandt, Igor V. Fomenkov, Nigel R. Farrar, Bruno La Fontaine, David W. Myers, Daniel J. Brown, Alex I. Ershov, Richard L. Sandstrom, Georgiy O. Vaschenko, Norbert R. Böwering, Palash Das, Vladimir B. Fleurov, Kevin Zhang, Shailendra N. Srivastava, Imtiaz Ahmad, Chirag Rajyaguru, Silvia De Dea, Wayne J. Dunstan, Peter Baumgart, Toshi Ishihara, Rod D. Simmons, Robert N. Jacques, Robert A. Bergstedt, Peter I. Porshnev, Christopher J. Wittak, Robert J. Rafac, Jonathan Grava, Alexander A. Schafgans, Yezheng Tao, Kay Hoffmann, Tedsuja Ishikawa, David R. Evans, Spencer D. Rich

Cymer Inc., 17075 Thornmint Court, San Diego, CA 92127, USA

ABSTRACT

Laser produced plasma (LPP) systems have been developed as the primary approach for use in EUV scanner light sources for optical imaging of circuit features at 20nm nodes and beyond. This paper provides a review of development progress and productization status for LPP extreme-ultra-violet (EUV) sources with performance goals targeted to meet specific requirements from ASML. We present the latest results on power generation and collector protection for sources in the field operating at 10W nominal power and in San Diego operating in MOPA (Master Oscillator Power Amplifier) Prepulse mode at higher powers. Semiconductor industry standards for reliability and source availability data are provided. In these proceedings we show results demonstrating validation of MOPA Prepulse operation at high dose-controlled power: 40 W average power with closed-loop active dose control meeting the requirement for dose stability, 55 W average power with closed-loop active dose control, and early collector protection tests to 4 billion pulses without loss of reflectivity.

Keywords: EUV source, EUV lithography, Laser Produced Plasma, Collector, Droplet Generator

1. INTRODUCTION

EUV Lithography is the front runner for next generation critical dimension imaging to replace 193 nm immersion lithography for critical layer patterning below the 22 nm node. Leading device manufacturers took delivery of first generation EUV sources in 2011 and have ramped those tools to pilot-line capability in 2012. The development of high power capability up to 250W and beyond for EUV sources is considered to be one of the critical challenges, along with other technologies such as resist and mask, for realization of EUV lithography in high volume. High sensitivity photoresists with good line-edge-roughness (LER) and line-width-roughness (LWR) are needed to keep the required source power within reasonable limits. Photoresist sensitivity and overall optical transmission through the EUV scanner are the basis to derive EUV source power requirements within the usable bandwidth of 2 %. ASML is requiring clean EUV power of 250W at the intermediate focus (IF) to enable > 100 wph scanner throughput assuming photoresist sensitivity of 15 mJ/cm².

LPP EUV lithography light sources generate the required 13.5 nm radiation by focusing a 10.6 micron wavelength CO₂ laser beam onto tin (Sn) droplet targets creating highly ionized plasmas with electron temperatures of several 10's of eV¹⁻⁴. EUV photons are radiated isotropically by these ions. Photons are collected with a temperature-controlled graded multilayer coated normal-incidence mirror (collector), and focused to an intermediate point from where they are relayed to the scanner optics and ultimately to the wafer. High conversion efficiency (CE) of the laser energy into EUV energy is critical to meeting the required power levels. The collector is protected from the plasma by a debris mitigation technology based on a hydrogen buffer gas. High-energy ions, fast neutrals, and residual source element particles are mitigated to maintain the reflectivity of the collector mirror and enable a long lifetime for this component. .

A total of ten HVM I sources have been built and are operational. Five of these sources are now installed at chipmaker R&D facilities and are being used to expose wafers for device production, three are used at Cymer in San Diego for development of upgrades and two are being used by ASML for continued development of the scanner modules. First source performance results including power and dose stability as well as initial testing were described a year ago^{5,6}. Collector lifetime in the field now exceeds 75 billion pulses, principally due to the development of new coatings and improved control of the vacuum environment. The source availability as defined by SEMI E10 is >65% average over the last three months. The increase in source availability is primarily due to the increase in lifetime of two critical modules; the collector and the droplet generator. Cymer has deployed service teams to support source operation, 7 days per week, 24 hours per day, in all locations where the sources are installed, which now includes Korea, Taiwan, Japan, USA and Europe. With the work now being complete for HVM I (3100), we have increased our focus on using the sources in our factory to develop and test power upgrades and availability enhancements. All three sources have been upgraded to MOPA Prepulse configuration by adding the master oscillator and Prepulse controls.

2. LPP SOURCE SYSTEM

The system architecture is shown in a scale drawing in Figure 1. The three major subsystems of the source are the drive laser, the beam transport system (BTS) and the source vessel. The drive laser is a CO₂ laser with multiple stages of amplification to reach the required power level of up to ~40 kW.⁷⁻⁹ It is operated in pulsed mode at ~50 kHz with radio-frequency (RF) pumping from generators (not shown) operating at 13.56 MHz. The laser is typically installed in the sub-fab along with its RF generators and water-to-water heat exchangers. The laser beam is expanded as it leaves the drive laser to lower the energy density on the BTS mirrors and to enable higher NA for focusing the beam to a small spot size. Turning mirrors are used to allow the beam to travel from the sub-fab to the fab through the waffle-slab floor with the needed flexibility for positioning the laser with respect to the source vessel (and scanner) on the floor above. The laser and BTS are completely enclosed and interlocked to meet laser class 1 requirements. The BTS delivers the beam to a focusing optic where the light at 10.6 μm wavelength is focused to a minimum spot size defined by the numerical aperture of the focusing system. The converging beam propagates through a central aperture in the collector and strikes the droplet at the primary focus of the ellipsoidal collector mirror inside the vacuum space of the source vessel. The droplet generator delivers liquid tin droplets of about 30 μm in diameter to the same position at

~50 kHz repetition rate; both laser pulse and droplets are steered and timed to ensure proper targeting. The laser pulse vaporizes and heats the tin into a plasma cloud of critical temperature and density. The EUV light emitted by the plasma is collected and reflected with the multilayer-coated ellipsoidal mirror to the IF where it passes through a small aperture into the scanner volume that houses the illumination optics.

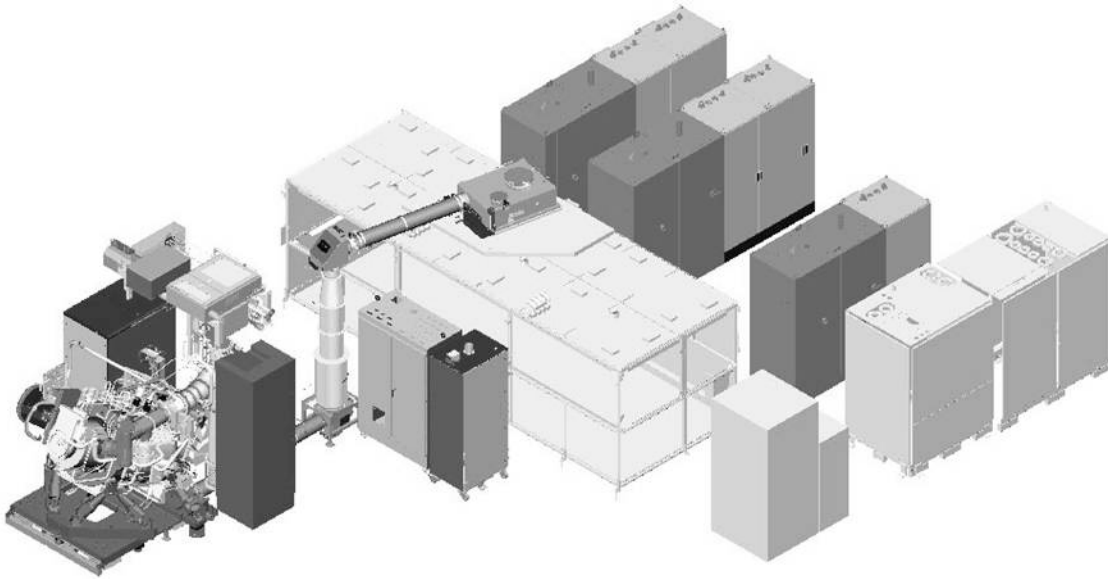


Figure 1: Scale Drawing of Laser Produced Plasma Source for ASML NXE:3100.

To ensure that no contamination can reach the scanner volume an IF protection module surrounds the aperture and suppresses flow and diffusion¹⁰. Other modules on the source vessel include the droplet catcher which collects the unused droplets between the bursts, and metrology modules used to measure EUV energy and to image droplets and plasma. The source controller turns on and off bursts of pulses as commanded by the scanner, which can be as long as several seconds. Full field exposures were tested with corresponding exposure timing for a 26 x 33mm field size using 15 – 20 mJ/cm² resist. The ratio of time when the burst is on to the period between bursts defines the inter-field duty cycle.

3. MOPA PREPULSE DEVELOPMENT RESULTS

Three test sources in San Diego have been upgraded to MOPA Prepulse mode of operation by adding oscillators for both main and prepulses to the front end of the drive laser. Isolation protection, optical switching, polarization control and metrology were also added. The control of Prepulse required a new high speed (100kHz) board, algorithms and software to enable the timing between pre and main pulses to be controlled to the required accuracy. Recent development activities have enabled several milestones to be achieved as part of the performance validation of 40W stable operation over long periods of time. The source was run for multiple hours over multiple days and demonstrated repeatable stable performance. 40W average EUV

power at IF in six 1-hour runs over 8.5-hours total operating time is shown in Figure 2a. The off-time between runs was used to demonstrate thermal cycling of the source and repeatable performance upon restarting. The dose stability for each of the 1-hour runs was better than $<\pm 0.2\%$, with the exception of one die in the fourth run, as shown in Figure 2b. The vertical line is an indication of this one bad die. However, it should be noted that this is a *low* energy exposure, and it may be feasible for the scanner to identify the location and return to add energy to this die as needed. The intrinsic baseline dose stability when no energy excursions are present is about $<\pm 0.1\%$; it represents the intrinsic capability of the source operating at 50kHz frequency.

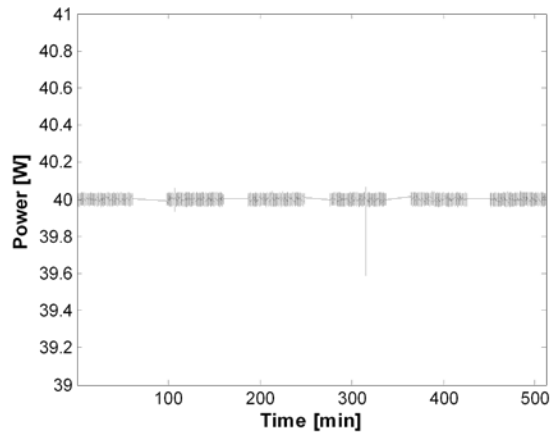


Figure 2a: 40W Average Power using MOPA Prepulse

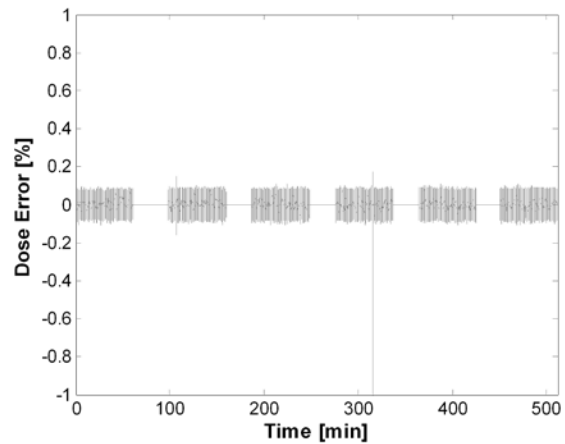


Figure 2b: 40W Dose Stability using MOPA Prepulse

The burst-to-burst dose stability can be seen when the time scale is expanded, as shown in Figure 3a. In this case, the source was running using 2 second die exposures at 100% duty cycle within the burst, and at 92% duty cycle burst-to-burst. The off-time between bursts represents the stepping time between die. A typical within wafer die yield distribution graph is shown in Figure 3b. In this example 100% of the dies yielded. Yield is defined as dose stability $<\pm 0.5\%$, but typical performance was much better and approached the intrinsic baseline stability of the source.

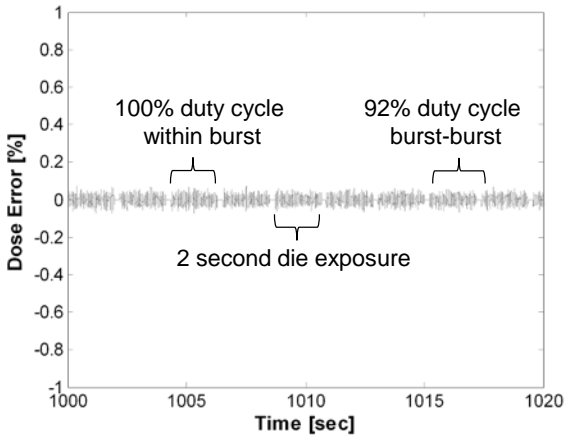


Figure 3a: 40W Dose Stability Burst-to-Burst

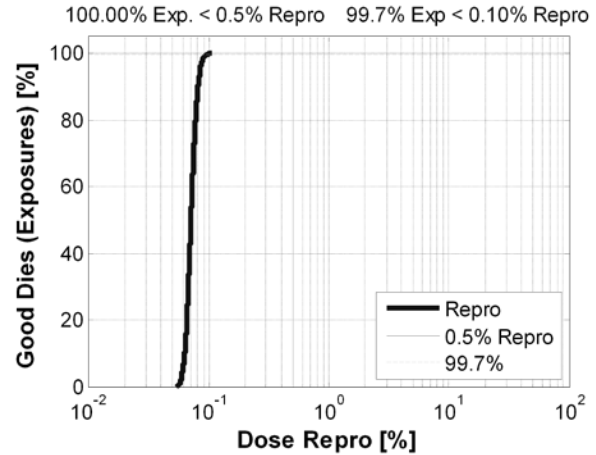


Figure 3b: 40W Die Yield

Because the stability of the source at 40W showed considerable performance margin the target power was increased to test the source at 55W, as shown in Figure 4a. A 1-hour run at 55W was achieved with only a small reduction of dose stability, as observed from the increased number of vertical lines representing energy excursions in the 55W data as compared to the 40W data. The die yield for this one 1-hour run at 55W was determined to be 97.5%. The Conversion Efficiency (CE) of a MOPA Prepulse source has been previously shown to approach 5% in low repetition rate laboratory experiments. Figure 4b shows >2% CE for a fully integrated system operating at full repetition rate of 50kHz in MOPA Prepulse. Optimization of CE will be used in future as one of the paths to increase power to meet roadmap requirements.

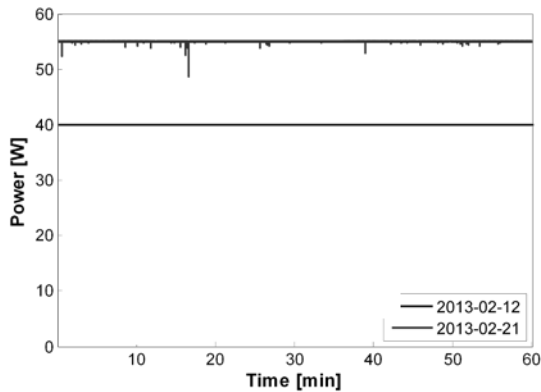


Figure 4a: 55W Average Power

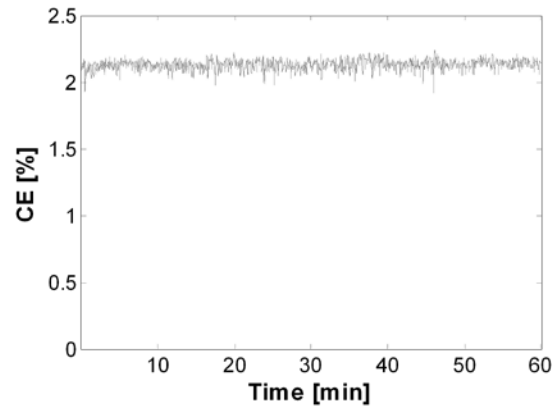


Figure 4b: 55W Conversion Efficiency (CE)

Collector lifetime is a critical parameter for the economic viability of an EUV source to be used in mass production of cost sensitive semiconductor devices. The 5sr multi-layer coated >650mm diameter ellipsoidal normal incidence collector must survive in the vacuum environment in the presence of a Sn plasma at a distance of ~200mm. Debris mitigation consisting of hydrogen gas at a given pressure and flow rate provides the protection needed to keep the optic clean and damage free over its lifetime. Figure 5a is the trend of relative reflectivity versus pulse count for

a collector in a 3100 source in the field operating at a nominal 10W. This collector has survived for greater than 8 months of operation (>75 billion pulses). This lifetime represents a ~10X improvement in lifetime since the first collectors were used in the 3100 source. New coating materials and improved control of the vacuum environment have enabled this level of performance.

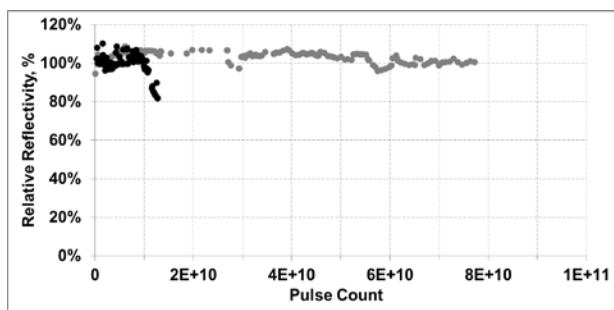


Figure 5a: Collector Lifetime in the Field >75 Billion Pulses

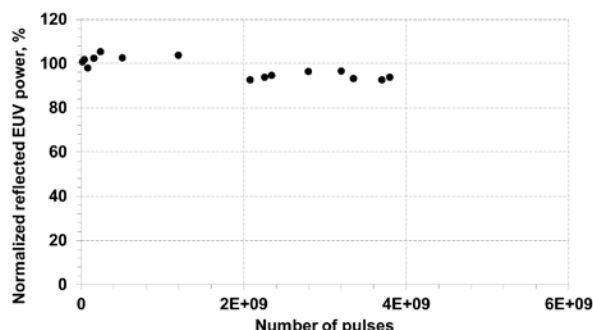


Figure 5b: MOPA Prepulse Collector Lifetime – Early Results Show no Degradation

The sources in San Diego are being used to test collector protection in MOPA Prepulse mode during operation at power levels much higher than currently used in the field. Figure 5b shows the normalized EUV power versus number of pulses for a collector test using recently optimized protection conditions and current vacuum cleanliness practices. The raw power (not under dose control) during this test started at 30W and was increased to 40W and then to 60W. The collector protection was determined to be effective since this number of pulses is sufficient to conclude that there are no new early damage mechanisms. Follow-on tests are planned up to 15 billion pulses and beyond.

4. ROADMAP

EUV Power is determined by input CO₂ laser power, conversion efficiency (CE) and collection efficiency. The increase in values for these parameters required for higher power output have been estimated and are shown in the roadmap in Figure 9 for 3300 sources. The first column shows the current high power result which represents our starting point. The goal for clean EUV power is 250W, achieved primarily through scaling CO₂ power and CE. LPP has been shown to be the scalable architecture needed to enable the evolution of EUV lithography during the life cycle of the technology. Laser-produced-plasma sources are expected to deliver the necessary power for critical-dimension high-volume manufacturing (HVM) scanners for the production of integrated circuits in the post-193 nm immersion lithography era.

	Pilot 9	3300: 80W	3300: 125W	3300: 250W
EUV dose controlled power (in-burst)	55W	80W	125W	250W
Duty Cycle (in-burst)	100%	100%	100%	100%
Drive Laser	15kW	24kW	31kW	43kW
CE	2%	2%	2%	3%

Figure 6: Projected LPP EUV Source Roadmap

5. SUMMARY

Laser-produced plasmas have been shown to be the leading source technology with scalability to meet requirements of ASML scanners and provide a path toward higher power needed by lithography tools as they evolve over their life cycle. Ten 3100 sources have been built and are operational around the world. Reliable operation of sources in the field have averaged >65% availability over the past 3 months.

MOPA Prepulse technology has been validated as the path to higher power output. Average power of 40W at intermediate focus over long bursts at 92% duty cycle has been demonstrated over long run times. The capability of meeting the dose stability target of $\leq \pm 0.2\%$ 3σ has been validated. Capability of 55W operation at high duty cycle was also demonstrated. Normal-incidence collector mirrors with > 5 sr light collection and high average reflectivity are being produced in volume and are showing increasingly long lifetimes in the field. 3300 sources are being built and shipped, and their integration into 3300 scanners has begun. Several sources will also be built for use as internal test sources at Cymer and at ASML.

ACKNOWLEDGEMENTS

The authors gratefully acknowledge the valuable contributions from Joost de Pee of ASML, Bob Lofgren, John Sporre and David N. Ruzic of University of Illinois, Urbana Champaign, Marco Perske, Hagen Pauer, Sergiy Yulin, Torsten Feigl, Norbert Kaiser and co-workers of Fraunhofer Institut f. Angewandte Optik und Feinmechanik, Eric Gullikson and Farhad Salmassi of Lawrence Berkeley National Laboratory, Frank Scholze, Christian Laubis, Christian Buchholz and coworkers at PTB, and Mark Tillack of the University of California at San Diego. We are also very thankful for the invaluable support and contributions, past and present, of many scientists, engineers and technicians involved in the EUV technology program at Cymer. Likewise, we are thankful to many colleagues at ASML for helpful discussions of various aspects related to the light source operation.

REFERENCES

- [1] Brandt, D.C., Fomenkov, I.V., Ershov, A.I., Partlo, W.N., Myers, D.W., Böwering, N.R., Farrar, N.R., Vaschenko, G.O., Khodykin, O.V., Bykanov, A.N., Hoffman, J.R., Chrobak, C.P., Srivastava, S.N., Ahmad, I., Rajyaguru, C., Golich, D.J., Vidusek, D.A., De Dea, S., Hou, R.R., in: *Proc. of SPIE Vol. 7271, Alternative Lithographic Technologies*, F. M. Schellenberg, B. M. La Fontaine, Eds., 727103, (2009).
- [2] Fomenkov, I.V., Brandt, D.C., Bykanov, A.N., Ershov, A.I., Partlo, W.N., Myers, D.W., Böwering, N.R., Farrar, N.R., Vaschenko, G.O., Khodykin, O.V., Hoffman, J.R., Chrobak, C.P., Srivastava,

S.N., Golich, D.J., Vidusek, D.A., De Dea, S., Hou, R.R., in: *Proc. of SPIE Vol. 7271, Alternative Lithographic Technologies*, F. M. Schellenberg, B. M. La Fontaine, Eds., 727138 (2009).

[3] Böwering, N.R., Fomenkov, I.V., Brandt, D.C., Bykanov, A.N., Ershov, A.I., Partlo, W.N., Myers, D.W., Farrar, N.R., Vaschenko, G.O., Khodykin, O.V., Hoffman, J.R., Chrobak, C.P., Srivastava, S.N., Ahmad, I., Rajyaguru, C., Golich, D.J., Vidusek, D.A., De Dea, S., Hou R.R., *Journal of Micro/Nanolith. MEMS MOEMS* 8(4), 041504 (2009).

[4] Brandt, D.C, Fomenkov, I.V., Ershov, A.I., Partlo, W.N., Myers, D.W., Sandstrom, R.L., La Fontaine, B.M., Lercel, M.J., Bykanov, A.N., Böwering, N.R., Vaschenko, G.O., Khodykin, O.V., Srivastava, S.N., Ahmad, I., Rajyaguru, C., Das, P., Fleurov, V.B., Zhang, K., Golich, D.J., De Dea, S., Hou, R.R., Dunstan, W.J., Wittak, C.J., Baumgart, P., Ishihara, T., Simmons, R.D., Jacques, R.N., Bergstedt, R.A., in: *Proc. of SPIE Vol. 7969, Extreme Ultraviolet (EUV) Lithography II*, B. M. La Fontaine, P. P. Naulleau, Eds., 79691H (2011).

[5] Brandt, D.C., Fomenkov, I.V., Lercel, M.J., La Fontaine, B.M., Myers, D.W., Brown, D.J., Ershov, A.I., Sandstrom, R.L., Bykanov, A.N., Vaschenko, G.O., Böwering, N.R., Das, P., Fleurov, V.B., Zhang, K., Srivastava, S.N., Ahmad, I., Rajyaguru, C., De Dea, S., Dunstan, W.J., Baumgart, P., Ishihara, T., Simmons, R.D., Jacques, R.N., Bergstedt, R.A., Porshnev, P.I., Wittak, C.J., Woolston, M.R., Rafac, R.J., Grava, J., Schafgans, A.A., Tao, Y., in: *Proc. SPIE Vol. 8322, Extreme Ultraviolet (EUV) Lithography III*, P. P. Naulleau, Obert R. Wood II, Eds., 83221I (2012).

[6] Fomenkov, I.V, Böwering, N.R., Brandt, D.C., Brown, D.J., Bykanov, A.N., Ershov, A.I., La Fontaine, B., Lercel, M.J., Myers, D.W., in: *Proc. SPIE Vol. 8322, Extreme Ultraviolet (EUV) Lithography III*, P. P. Naulleau, Obert R. Wood II, Eds., 83222N (2012).

[7] Brandt, D.C., Fomenkov, I.V., Ershov, A.I., Partlo, W.N., Myers, D.W., Böwering, N.R., Bykanov, A.N., Vaschenko, G.O., Khodykin, O.V., Hoffmann, J. R., Vargas E.L., Simmons, R.D., Chavez, J.A., Chrobak, C.P., in: *Proc. of SPIE Vol. 6517, Emerging Lithographic Technologies XI*, M. J. Lercel, ED., 65170Q (2007).

[8] Fomenkov, I.V., Hansson, B.A.M., Böwering, N.R., Ershov, A.I., Partlo, W.N., Fleurov, V.B., Khodykin, O.V., Bykanov, A.N., Rettig, C.L., Hoffman, J.R., Vargas E.L., Chavez, J.A., Marx, W.F., Brandt, D.C., in: *Proc. of SPIE Vol. 6151, Emerging Lithographic Technologies X*, M. J. Lercel, Ed., 61513X (2006).

[9] Fomenkov, I.V., Brandt, D.C., Bykanov, A.N., Ershov, A.I., Partlo, W.N., Myers, D.W., Böwering, N.R., Vaschenko, G.O., Khodykin, O.V., Hoffman, J.R., Vargas, E., L., Simmons, R.D., Chavez, J.A., Chrobak, C.P., in: *Proc. of SPIE Vol. 6517, Emerging Lithographic Technologies XI*, M. J. Lercel, ED., 65173J (2007).

[10] Fomenkov, I.V., Ershov, A.I., Partlo, W.N., Myers, D.W., Brown, D., Sandstrom, R.L., La Fontaine, B.M., Bykanov, A.N., Vaschenko, G.O., Khodykin, O.V., Böwering, N.R., Das, P., Fleurov, V.B., Zhang, K., Srivastava, S.N., Ahmad, I., Rajyaguru, C., De Dea, S., Hou, R.R., Dunstan, W.J., Baumgart, P., Ishihara, T., Simmons, R.D., Jacques, R.N., Bergstedt, R.A., Brandt, D.C., in: *Proc. of SPIE Vol. 7969, Extreme Ultraviolet (EUV) Lithography II*, B. M. La Fontaine, P. P. Naulleau, Eds., 796933 (2011).

High Power 120W ArF immersion XLR laser system for high dose applications

R. Rokitski, R. Rafac, J. Melchior, R. Dubi, J. Thornes, T. Cacouris, M. Haviland, D. Brown,
Cymer, Inc. (United States)

ABSTRACT

Demand for increased semiconductor device performance at low cost continues to drive the requirements for shrinking the geometry of features printed on silicon wafers. Argon fluoride (ArF) excimer laser systems operating at 193 nm and producing high output power played a key role in patterning of the most advanced features for high volume deep ultraviolet (DUV) lithography over the last decade. Lithographic patterning has progressed from ArF dry to ArF immersion (ArFi) to double and multiple patterning applications, with increasingly tight requirements for the quality of light at 193 nm and improved system reliability. This drove the transition from single chamber laser systems to dual chamber systems with ring cavity amplifier architectures. We are presenting a flexible 90-120W ArFi excimer laser system, developed for high volume multiple patterning manufacturing as well as 450mm wafer applications. Light source design is based on dual-chamber architecture with ring cavity power amplifier.

1. INTRODUCTION

Since their first introduction in 2007 [1] XLR laser systems with ring cavity amplifier architecture established a proven track record due to their excellent performance. Flexibility and high reliability of these light sources is continuously demonstrated under diverse operating conditions of most advanced lithographic patterning applications. The range of applications of XLR 600ix systems extends from ArF dry to multi-patterning immersion lithography, including high dose and enhanced depth of focus applications for contact hole patterning [2,3].

Further advancement of the DUV lithography to 2x - 1x nm nodes and cost reduction drives increased scanner wafer stage speed and transition to 450mm wafer size. This transition requires additional power from the light source and a larger range of system duty cycle. It imposes tighter requirements on system stability as the number of pulses within an exposure window is reduced. System reliability and availability under the more stringent and challenging set of operating conditions is expected to meet or exceed the levels demonstrated by 60W and 90W laser systems in high volume manufacturing environments [3].

We are reporting on development of XLR 600ix-HP, a flexible 90-120W light source for future high volume DUV lithography applications. Based on the flexible 60-90W architecture of XLR 600ix with high performance and reliability record, the XLR 600ix-HP delivers improved performance to meet the requirements for high dose application and support the transition to 450mm wafer size. System output power, operating wavelength and spectral bandwidth of XLR 600ix-HP can be varied in a wide range for each wafer, providing flexible system operation under diverse lithography process conditions.

2. XLR TECHNOLOGY ADVANCEMENT FOR 120W OPERATION

Excimer laser systems employed in semiconductor industry for high volume manufacturing produce light in the form of pulses with pulse duration in the 60-150 ns range and typical energy of 5-20 mJ per pulse. The combined energy of multiple pulses delivered per unit area of semiconductor wafer is used for photoresist exposure. Light sources with 60 and 90W output power produce pulses with 10 and 15 mJ nominal energy respectively. Higher output power of the laser system is achievable either through increased pulse repetition rate or by increasing the energy of every pulse. In our laser

system design 120W output power is achieved by increasing nominal pulse energy from 10-15 mJ to 15-20 mJ, while maintaining the range of pulse repetition rates.

Development of powerful and reliable light sources at 193 nm wavelength historically represented a significant technological challenge. The vast majority of the commonly used optical materials degrade under exposure to high peak fluence 193 nm light. Calcium fluoride (CaF_2) is typically used for transmissive elements inside the light source due to its excellent optical properties. Despite its relative robustness, when compared to other optical materials, CaF_2 surface and bulk is damaged under continuous exposure, typical for uninterrupted light source operation in high volume semiconductor manufacturing environment. This damage to optical component material ultimately limits module lifetime and can have a negative effect on light source mean time between interrupts (MTBI), increasing the cost of ownership.

When compared to beam delivery, illumination and projection lithographic systems, the risk of material damage is significantly higher inside the excimer light source due to high peak fluence of the optical beam. Optical components inside the light source are subject to significantly higher optical power of the beam with substantially shorter pulse duration and beam size. Damage to CaF_2 components can occur in bulk material via calcium colloid formation [4] and on the surface through calcium fluoride conversion to calcium carbonate [5]. These damage mechanisms are being addressed by material and component manufacturers to support long component lifetime at elevated pulse energies.

In addition to optical material damage due to increased pulse energy, thermally induced lensing and birefringence effects can be observed at elevated power load on the light source optical components. These phenomena can cause variation of beam polarization, near and far field profile with laser duty cycle. With tight requirements for the light source performance under all operating conditions, thermally induced birefringence and thermal lensing need to be addressed with output power level increased to 120W. We've addressed these potential issues in 120W light source by a combination of optical and mechanical component improvement as well as optical material selection for extended life time. An outcome of this effort is demonstrated as reduced sensitivity of output beam parameters to operating duty cycle as shown in Figs 1-3.

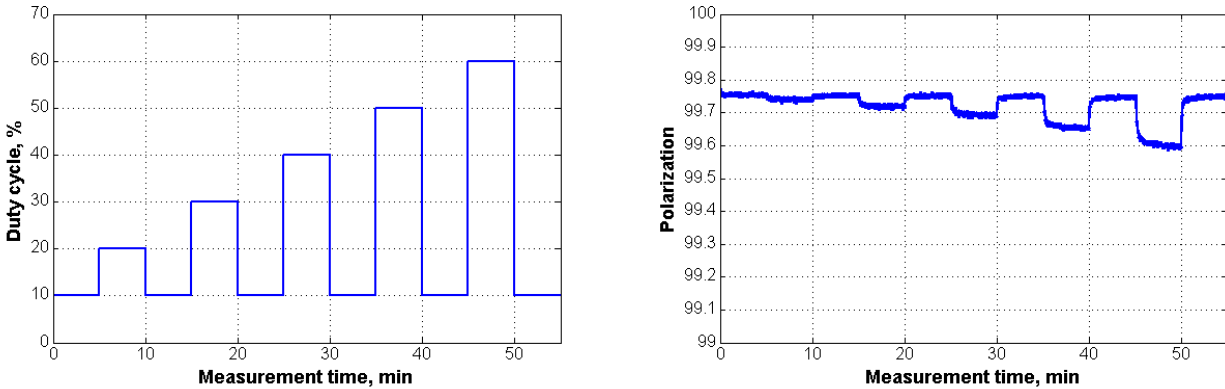


Fig. 1: 120W laser system duty cycle and output beam polarization, measured at 6 kHz, 20 mJ output pulse energy

Stability of all near and far field parameters of the output beam and polarization is very important for maintaining stable illumination conditions during wafer exposure. Beam parameter performance of the system, operating at 20 mJ output pulse energy, 6 kHz pulse repetition rate was evaluated at various duty cycles, as shown in Fig. 1. Output polarization stayed in a narrow range of 99.5-99.8% at all duty cycles, showing no significant effects of thermally induced

birefringence. Far field and near field parameters of the output beam show little dependence to the duty cycle of the system, indicating stable performance of the system. Low dependence of the beam parameters on output power level as shown in Fig. 1-3 ensures minimal contribution of the light source to wafer illumination.

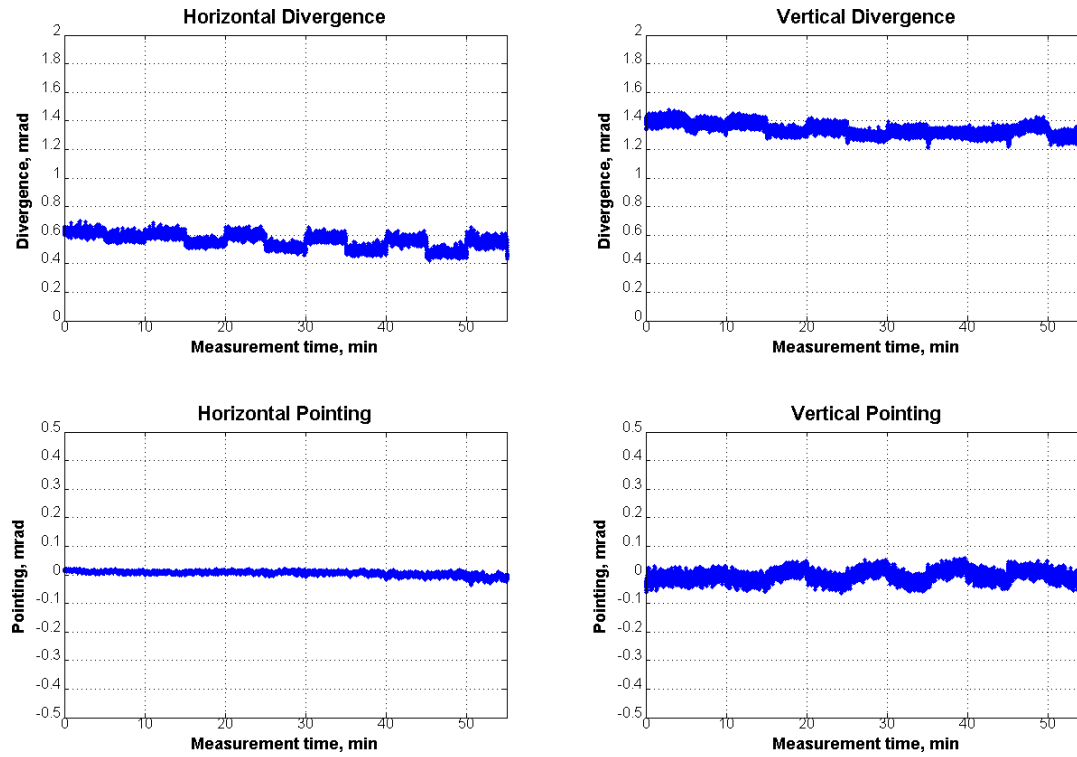


Fig. 2: Far field performance parameters of the 120W laser system, operating at 6 kHz, 10-60% duty cycle

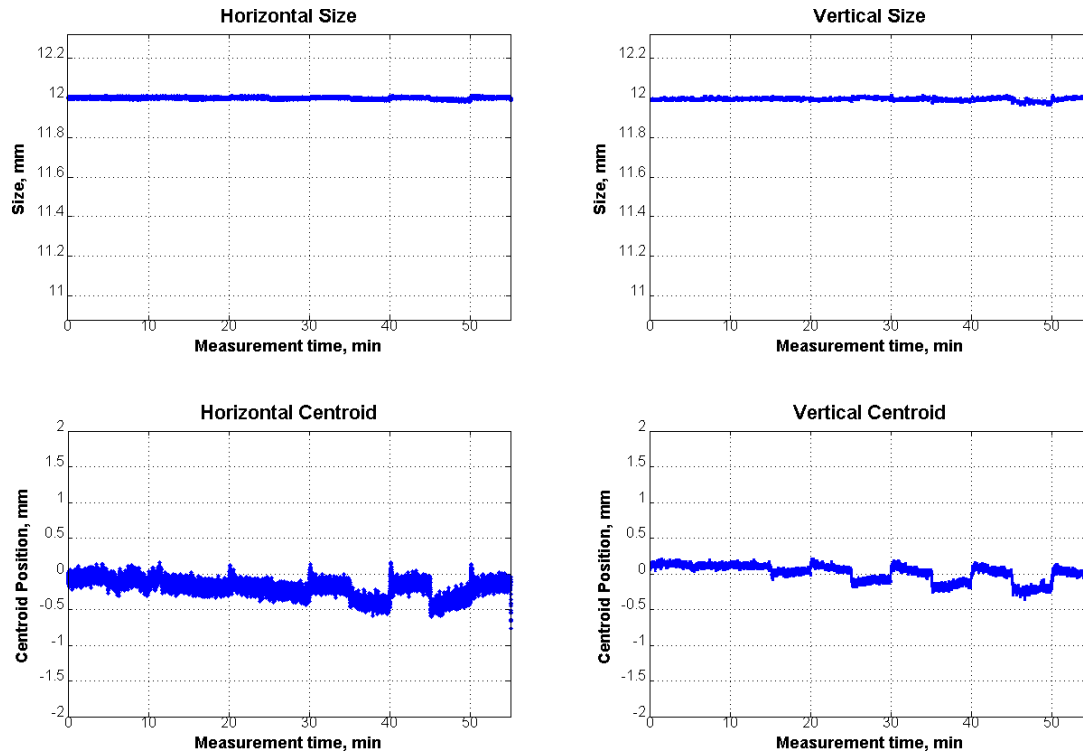


Fig. 3: Near field performance parameters of the 120W laser system, operating at 6 kHz, 10-60% duty cycle

3. SYSTEM PERFORMANCE WITH FAST 90/120W POWER SWITCHING

Fast power switching between 90 and 120W of the next generation XLR 600ix system is achieved by modulation of the losses in the ring power amplifier using intracavity attenuating elements. This approach allows the master oscillator (MO) subsystem of the light source to operate under the same conditions at 90 and 120W, reducing disturbances on output performance parameters associated with master oscillator. The power ring amplifier gain element operates under the same conditions at 90 and 120W as well, resulting in reduced transient effects when dose is changed significantly between wafers or wafer lots.

To evaluate stability of the system performance parameters under various operating conditions and output power levels we perform a stress test, where output pulse energy is varied in the range of 11.6 – 23 mJ and pulse repetition rate is changed between 1500 and 6000 Hz. These test conditions cover majority of the use cases, observed during system use in high volume manufacturing environment.

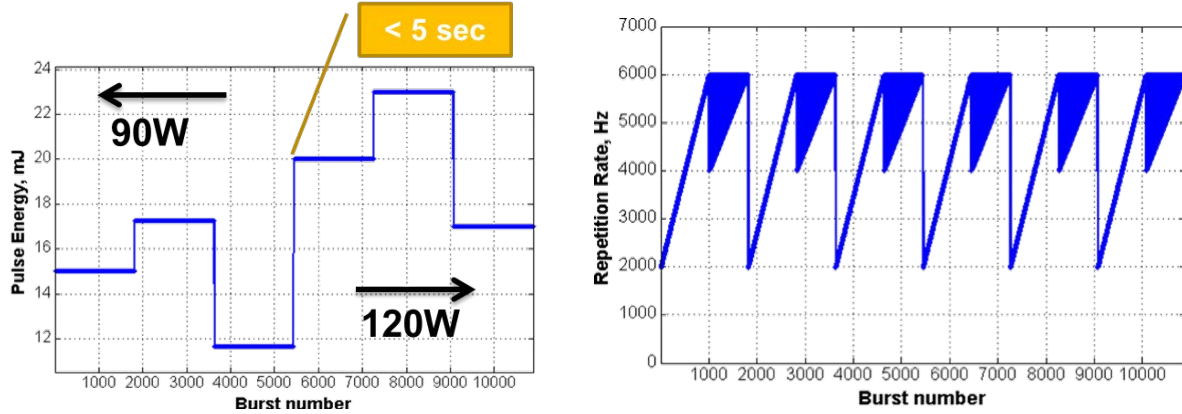


Fig. 4: Light source operating conditions during a performance stress test with fast power switching. Nominal power is switched from 90 to 120W during the test, simulating a wafer/lot exchange

In addition to the near and far field parameters of the beam contributing to illumination conditions, energy, wavelength and spectral bandwidth can have direct impact on dose, focus and CDU performance. With increased scanner stage speed, requirements on stability of these parameters are tighter, as a smaller number of pulses is being used to expose unit area on wafer. XLR 600ix laser systems historically demonstrated excellent stability of dose, wavelength and bandwidth E95. At increased output power and reduced integration window size, this performance level is maintained under all operating conditions.

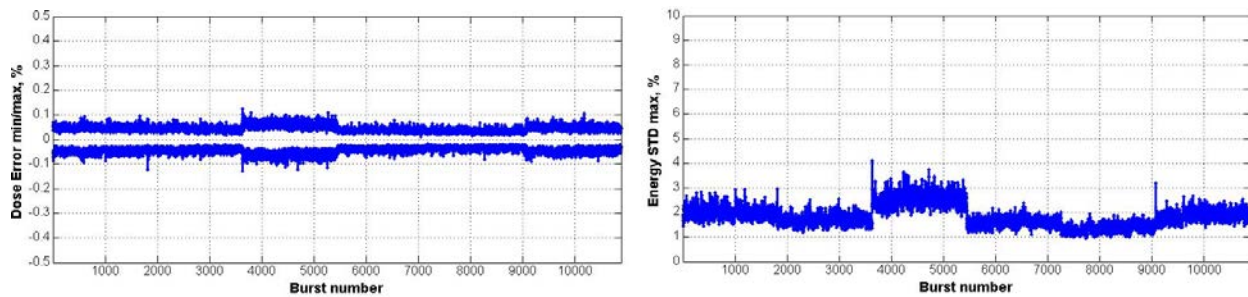


Fig.5: Dose and energy stability performance of the laser system at 90 and 120W nominal output power settings during the stress test

Excellent dose stability with reduced integration window size as shown in Fig. 5 satisfies performance requirements of the lithographic tools under all pulse repetition rates and energy settings. We did not observe significant dependence of energy stability on the output power range setting.

Focus stability of the image projected on the wafer can be affected by variation in the light source wavelength via chromatic aberrations in the scanner projection optics. To support stable focus the light source has to maintain wavelength stability within a tight range under all operating conditions, including different power settings and repetition

rates. In Fig. 6 we show that wavelength stability of the 120W light source remains undisturbed with nominal power and energy target setting.

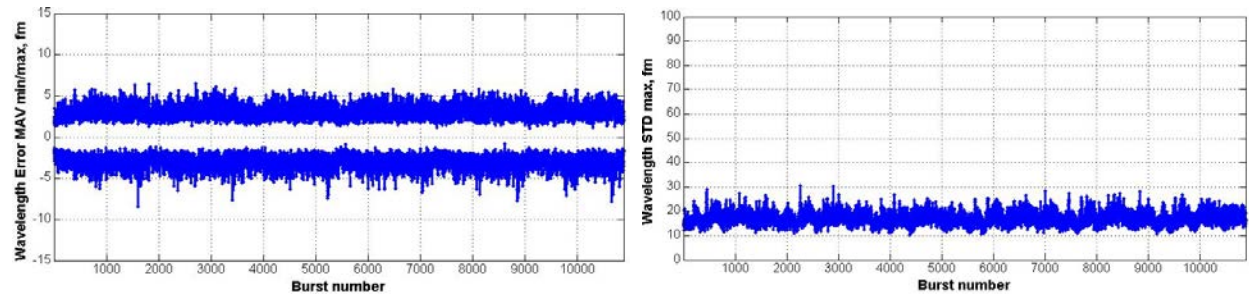


Fig.6: Wavelength stability performance of the laser system at 90 and 120W nominal output power settings during the stress test

Bandwidth E95 is another important parameter affecting uniformity of critical dimension (CD) of the features etched on semiconductor wafers. It represents spectral width of the light source output light with 95% of the total energy. We evaluated stability of bandwidth E95 during the stress test described above as well as during the repetition rate tests in wide range of energy and bandwidth E95 targets. Results of these tests, shown in Fig. 7, demonstrate excellent stability of bandwidth E95 in wide range of bandwidth targets, supporting matching of CDU for different lithographic tools.

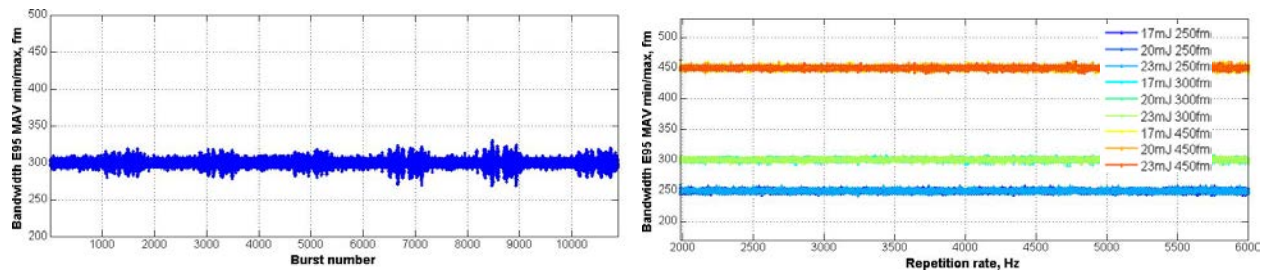


Fig.7: Bandwidth E95 stability performance of the laser system at 90 and 120W nominal output power settings during the stress tests

4. CONCLUSIONS

Dual chamber argon fluoride laser systems, operating at 193 nm play an important role in enabling continuous reduction of semiconductor node size. XLR light sources with output power in the 60-90 Watt range meet the requirements of diverse lithographic applications, ranging from ArF dry to ArF immersion multi-patterning. Further improvements in system throughput for cost effective manufacturing are enabled by XLR 600ix-HP laser systems with output power in a 90-120W range while meeting tighter performance requirements at increased scanner stage speed. We reported on excellent performance of XLR 600ix-HP system at 90 and 120W output power, developed to support extension of DUV lithography to 2x nm and beyond.

5. REFERENCES

1. D.J. W. Brown et al. "XLR 500i: recirculating ring ArF light source for immersion lithography", Proc. SPIE Vol. 6520, Optical Microlithography XX, 2007
2. R. Rokitski et al., "Enabling high volume manufacturing of double patterning immersion lithography with the XLR 600ix ArF light source", Proc. SPIE, Vol. 7274 Optical Microlithography XXII, 2009
3. T. Cacouris et al., "Advanced light source technologies that enable high-volume manufacturing of DUV lithography extensions", Proc. SPIE Vol. 8326 Optical Microlithography XXV, 2012
4. U. Natura et al, "Study of haze in 193 nm high dose irradiated CaF₂ crystals", Proc. SPIE Vol. 7504, 2009
5. M. Bauer et al, "Exterior surface damage of calcium fluoride outcoupling mirrors for DUV lasers", Optics Express Vol. 17, No. 10, 2009

Laser Produced Plasma EUV Light Source for EUVL Patterning at 20nm Node and Beyond

Igor V. Fomenkov, David C. Brandt, Nigel R. Farrar, Bruno La Fontaine
Norbert R. Böwering, Daniel J. Brown, Alex I. Ershov, David W. Myers

Cymer Inc., 17075 Thornmint Court, San Diego, CA 92127, USA

ABSTRACT

This paper describes the development of a laser-produced-plasma (LPP) extreme-ultraviolet (EUV) source for advanced lithography applications in high volume manufacturing. EUV lithography is expected to succeed 193nm immersion double patterning technology for sub-20nm critical layer patterning. In this paper we discuss the most recent results from high power testing on our development systems in San Diego, and describe the requirements and technical challenges related to successful implementation of these technologies. Subsystem performance will be shown including the CO₂ drive laser, droplet generation, laser-to-droplet targeting control, intermediate-focus (IF) metrology, out-of-band (OOB) radiation measurements and system use and experience. In addition, a multitude of smaller lab-scale experimental systems have also been constructed and tested..

Keywords: EUV source, EUV lithography, laser-produced plasma, collector, droplet generator

1. INTRODUCTION

At Cymer, we are engaged in the development of second generation LPP light sources providing the intense extreme ultraviolet (EUV) radiation required for next generation lithography scanners. A high-power CO₂ laser is focused onto tin (Sn) droplets creating a highly ionized plasma to emit the EUV radiation at wavelengths of around 13.5 nm. Different aspects and performance characteristics of our sources as well as related research and development progress at our facility were already described in detail in several earlier publications.¹⁻⁵ Last year we described initial dose stability results, power scaling and availability data for 3100 first-generation sources^{6,7} and also reported several new development results⁸. In addition to a prototype, 10 first-generation sources have been built and tested; most systems were deployed to customers for use in process development at early adopters of EUV lithography technology. As these EUV sources have now been in operation for approximately two years, further development is taking place in parallel to manufacturing of second generation sources in order to provide improvements to the average power and the availability of these sources for their users. In this paper we report on the characterization of source components that are critical to achieve the higher power and availability required for this first generation of light sources to support EUV scanners at chipmaker R&D facilities, and for technology transfer to the second generation of EUV sources.

2. SOURCE VESSEL CHANGES FROM 3100 TO 3300

Our LPP source architecture has three major subsystems: Drive Laser, Beam Transport System (BTS) and the Source Vessel. Significant design improvements have been made to the second generation source vessel as shown in Figure 1. These changes were specifically designed to enable higher power, greater stability and increased availability of the source. The source orientation angle was increased from 27 degrees to 62 degrees to provide a steeper angle of incidence of the light onto the first multi-layer mirror (MLM) in the illuminator; this in turn enabled the reduction of optical surfaces in the illumination section which increased the optical transmission of the entire system. The mass of the vessel was increased to provide improved stability under high thermal load. The mounting of metrology modules such as cameras and sensors was modified such that they are all attached to a common metrology external frame. Since the cameras are part of the control system to read positional stability of the droplet or laser beam, their motion contributes to the overall dose error in the system. The collector exchange process was significantly improved by adding a side port such that the collector is removed with a drawer and cart from the side; this change will allow a 10X reduction of downtime associated with the collector exchange.

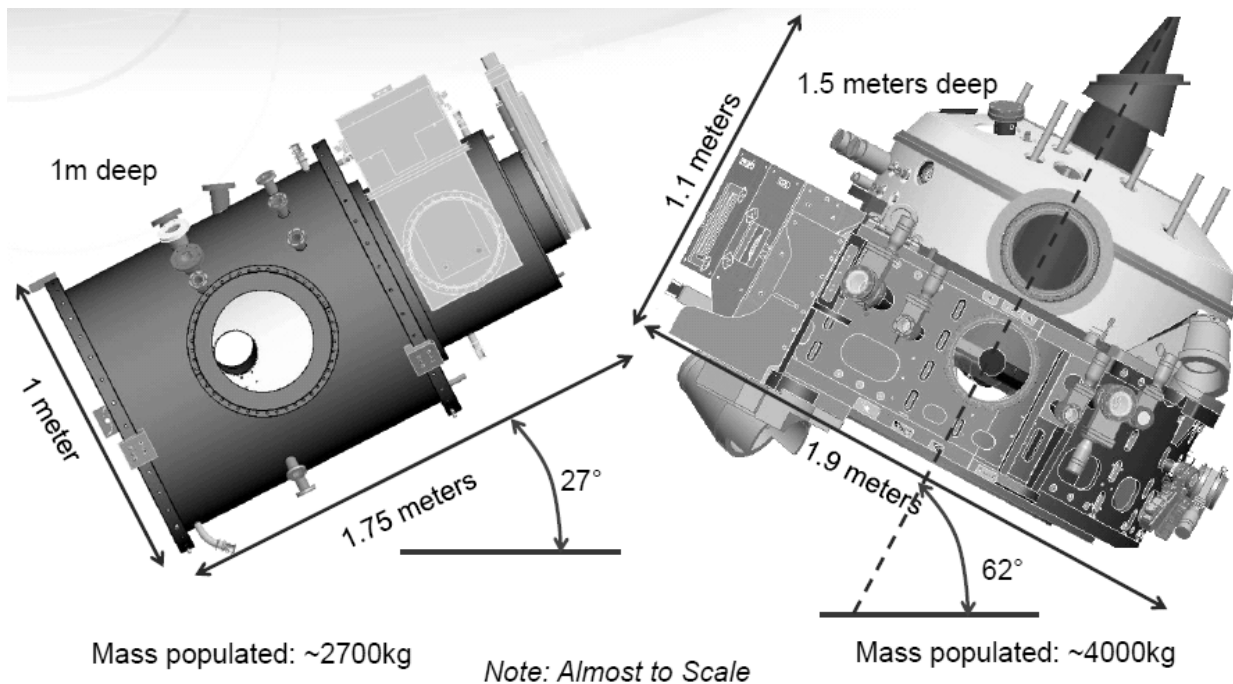


Figure 1: 3100 Source Vessel (shown on left), 3300 Source Vessel (shown on right).

Other changes include symmetric pumping of the hydrogen gas, improved routing of water lines and control cables, and an increased number of ports for additional metrology.

3. DEBRIS MITIGATION

Normal operation of the source produces a cleaning of Sn from the surface of the MLM coated collector. Tin vapor from the plasma expands to a uniform density inside the vacuum environment of the source vessel. All surfaces inside the vessel are designed to capture (or getter) tin such that no secondary transport occurs. The MLM coated surface of the collector must be kept free of tin deposition. Hydrogen gas is used as the primary mechanism for collector protection. As previously described⁸, this gas provides two forms of protection: First, the gas pressure between the plasma and the MLM surface stops fast ions and high energy particles and prevents them from reaching the collector surface and damaging the coating. Second, the hydrogen gas at the MLM surface is disassociated by ultraviolet radiation from the plasma into hydrogen radicals; these radicals react with tin to form Stannane (SnH_4), which is volatile and is thus carried away from the MLM surface with the flow of gas. The Stannane disassociates quickly, therefore it is important to rapidly sweep it away from the collector surface.

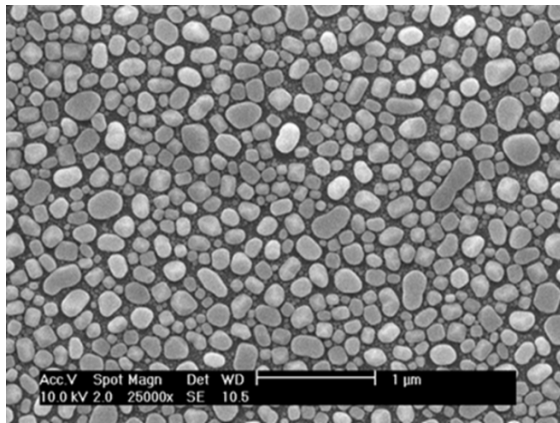


Figure 2a: SEM image of sample before installation into source chamber with 32 nm thick layer of tin deposited

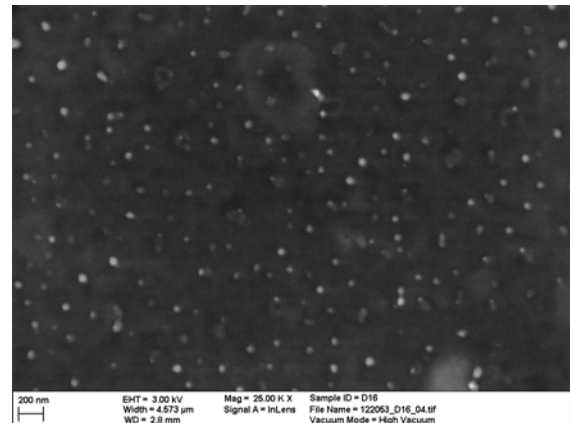


Figure 2b: SEM image of sample after source operation, thickness of tin is 2 nm, measured with X-Ray Fluorescence (XRF)

The cleaning of tin by this mechanism can be seen in Figures 2a and 2b which shows scanning electron microscopy (SEM) images of a coated test sample. A MLM sample with a 32 nm thick tin deposition was put onto sample holder inside of the vessel, the source was operated under normal conditions, and the average thickness of the tin layer was found to be reduced to 2 nm.

4. PARALLEL TESTING OF MLM COATED SAMPLES

An aluminum sample holder for multiple MLM samples was made to the specifications of the 5sr normal incidence collector for installation into a 3100 source. The second revision to the sample holder increased the number of sample sites from 54 to 92 to allow more coating materials to be tested in parallel during each run of the source.

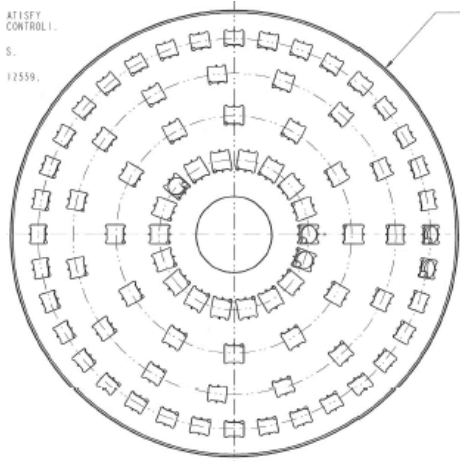


Figure 3a: MLM sample holder with 92 sites

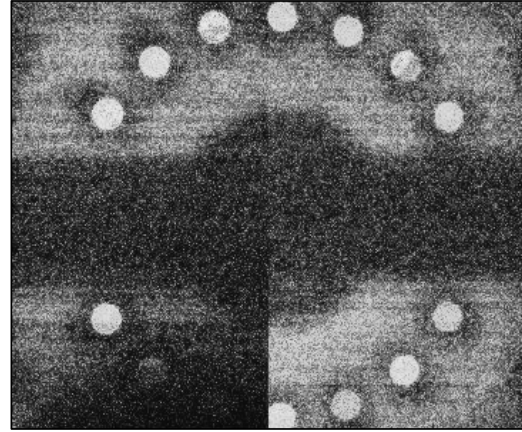


Figure 3b: Far-field EUV image of MLM samples under test

The MLM coating on the collector reported as reaching >75 billion pulses in the field⁶ was first tested and determined to have a significantly increased lifetime on the first version sample holder described above in a 3100 LPP test source at in our R&D facility in San Diego. The next significant improvement in collector lifetime is likely to be discovered on the new 92-sample massively parallel test apparatus, as shown in Figure 3a. During the operation of the source the sample reflectivity can be viewed in EUV light in the far field using the previously described⁸ Far-Field-Test-Tool (FTTT), as shown in Figure 3b.

5. HIGH SPEED DROPLETS

The development of higher speed tin droplet targets is required to enable stability of droplet position to support higher EUV power. The droplet generator developed by Cymer over the past seven years is now used on all sources globally 7 days a week, 24 hours a day. This device has undergone extensive development and engineering to bring the performance and reliability to the level we have today. Current performance is nominally: 30 micron droplet diameter, 60 m/s droplet velocity, 1 mm droplet spacing, 90% droplet generator start-up yield and 200hr droplet generator run time. Evolution of the droplet generator design includes operation at higher pressure to increase the speed of the droplets. Testing in our laboratory has already demonstrated stable performance at 28 micron diameter, 105 m/s velocity and 1.4 mm spacing of the droplets with no degradation of stability, as shown in Figure 4. The images and stability measurements were taken on a test bench in a vacuum vessel at a distance equal to the normal design parameters for the droplet generator nozzle to plasma site. Images are taken with a high

speed camera that allows post processing of the images to determine the stability of droplet position.

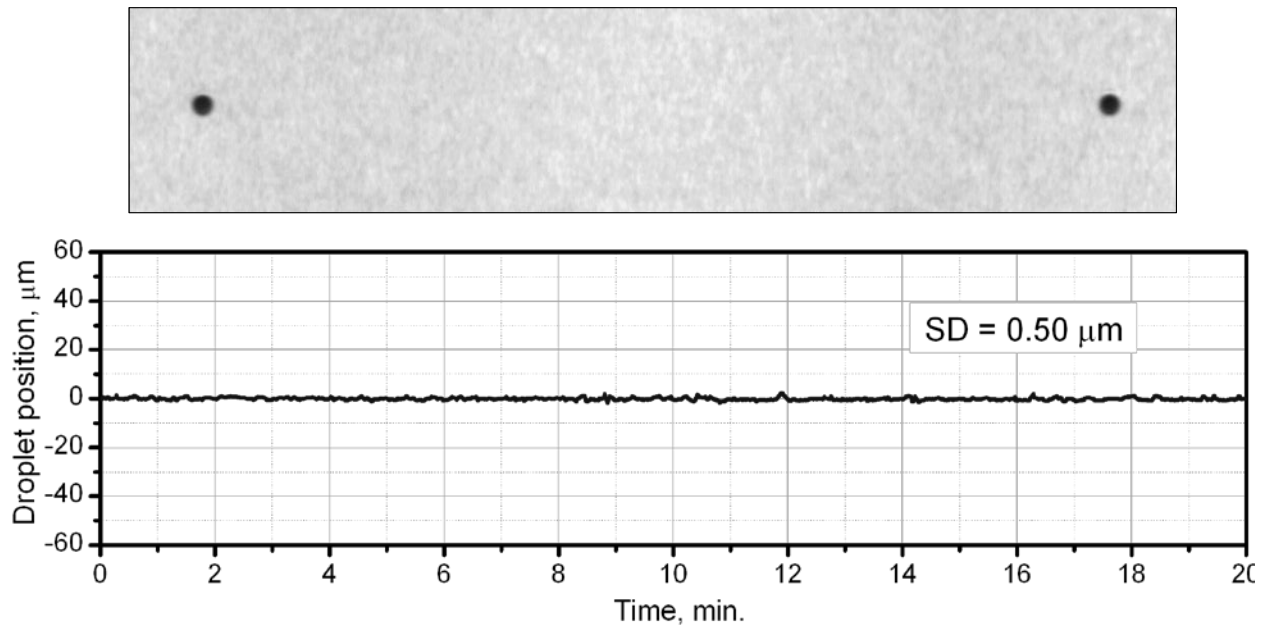


Figure 4: Droplet generation speed 105 m/s, frequency 75 kHz , diameter 28 μm , droplet-to-droplet distance 1.4 mm

6. OUT OF BAND RADIATION

Out-of-band (OOB) radiation was measured in MOPA Prepulse mode of operation using a grating spectrometer with a fiber pick-off looking through a fused silica window directly at the plasma. An Ocean Optics spectrometer was used to take the measurements; a calibration curve of responsivity versus wavelength was provided by the manufacturer of the spectrometer. The OOB region of interest for these measurements was the deep ultra-violet (DUV) range from 200nm to 300nm, as these wavelengths could potentially expose the photoresist (CAR type) and blur the image. These are the first measurements taken of the OOB radiation in a Sn/CO₂ LPP source during MOPA Prepulse operation.

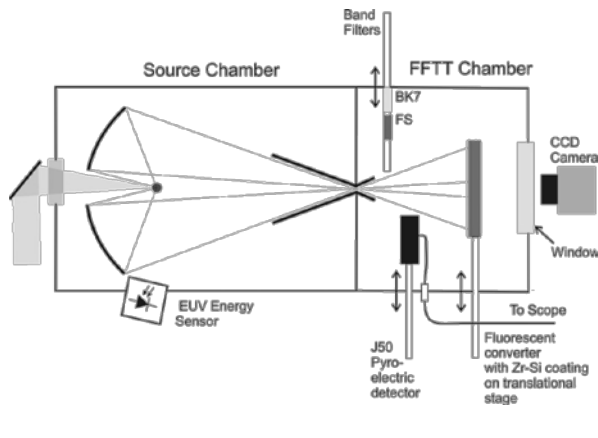


Figure 5a: Schematic of source vessel attached to FFTT

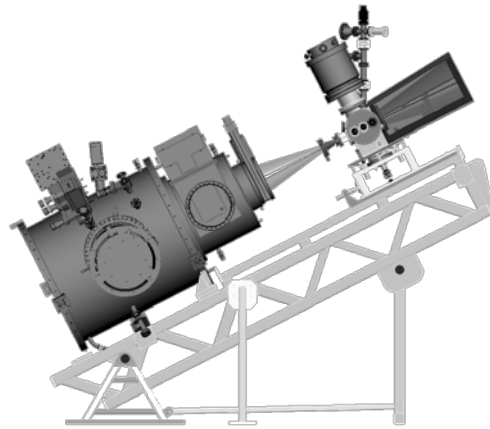


Figure 5b: 3100 Vessel with FFTT attached behind IF

The OOB measurements were taken on a 3100 source operating in MOPA Prepulse mode at an open loop raw power level of $\sim 100\text{W}$ in the burst, or 4.5 mJ per pulse into $2\pi\text{ sr}$. The DUV content (200 to 300nm) was measured to be approximately 2% of the EUV energy content. The spectrum emitted from the plasma in the wavelength range of 200 nm to 1000 nm is shown in Figure 6 together with the spectral integral.

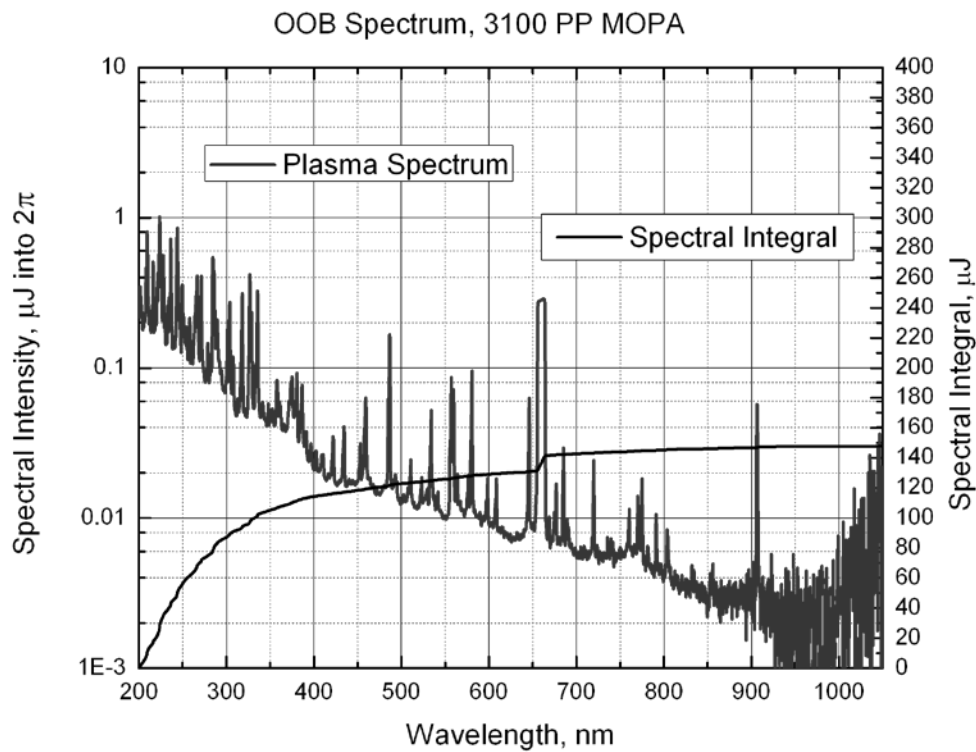


Figure 6: OOB Plasma Spectrum in MOPA Prepulse

7. SUMMARY

Second generation sources have been developed with improvements in drive laser power, conversion efficiency, availability and overall optical transmission. These sources are now shipping to ASML for the NXE:3300B EUV scanner. Normal operation of LPP sources provides cleaning of tin from the collector via hydrogen radicals and a high flow rate through the source vessel. MLM coating development is accelerated with the use of parallel sample testing on our LPP sources in San Diego. High speed droplets have been developed for the 250W source power node on the roadmap. Out-of-band radiation in the DUV band from 200 to 300 nm has been reported to be 2% of the EUV energy content.

ACKNOWLEDGMENTS

The authors gratefully acknowledge the invaluable support and contributions, past and present, of many scientists, engineers and technicians involved in the EUV technology program at Cymer. We also thank our colleagues at ASML for many helpful discussions of various aspects related to the light source operation.

REFERENCES

- [1] D. C. Brandt, I. V. Fomenkov, A. I. Ershov, W. N. Partlo, D. W. Myers, N. R. Böwering, N. R. Farrar, G. O. Vaschenko, O. V. Khodykin, A. N. Bykanov, J. R. Hoffman, C. P. Chrobak, S. N. Srivastava, I. Ahmad, C. Rajyaguru, D.J. Golich, D. A. Vidusek, S. De Dea, R. R. Hou, Proc. SPIE **7271**, 727103 (2009).
- [2] N. R. Böwering, I. V. Fomenkov, D. C. Brandt, A. N. Bykanov, A. I. Ershov, W. N. Partlo, D. W. Myers, N. R. Farrar, G. O. Vaschenko, O. V. Khodykin, J. R. Hoffman, C. P. Chrobak, S. N. Srivastava, I. Ahmad, C. Rajyaguru, D.J. Golich, D. A. Vidusek, S. De Dea, R. R. Hou, Journal of Micro/Nanolith. MEMS MOEMS 8(4), 041504 (2009).
- [3] D. C. Brandt, I. V. Fomenkov, A. I. Ershov, W. N. Partlo, D. W. Myers, R. L. Sandstrom, N. R. Böwering, G. O. Vaschenko, O. V. Khodykin, A. N. Bykanov, S. N. Srivastava, I. Ahmad, C. Rajyaguru, D. J. Golich, S. De Dea, R. R. Hou, K. M. O'Brien, W. J. Dunstan, Proc. SPIE **7636**, 76361I (2010).
- [4] I. V. Fomenkov, A. I. Ershov, W. N. Partlo, D. W. Myers, R. L. Sandstrom, N. R. Böwering, G. O. Vaschenko, O. V. Khodykin, A. N. Bykanov, S. N. Srivastava, I. Ahmad, C. Rajyaguru, D. J. Golich, S. De Dea, R. R. Hou, K. M. O'Brien, W. J. Dunstan, D. C. Brandt, Proc. SPIE **7636**, 763639 (2010).
- [5] I. V. Fomenkov, A. I. Ershov, W. N. Partlo, D. W. Myers, D. Brown, R. L. Sandstrom, B. M. La Fontaine, A. N. Bykanov, G. O. Vaschenko, O. V. Khodykin, N. R. Böwering, P. Das, V. B. Fleurov, K. Zhang, S. N. Srivastava, I. Ahmad, C. Rajyaguru, S. De Dea, R. R. Hou, W. J. Dunstan, P. Baumgart, T. Ishihara, R. D. Simmons, R. N. Jacques, R. A. Bergstedt, D. C. Brandt, Proc. SPIE **7969**, 796933 (2011).
- [6] D. C. Brandt, I. V. Fomenkov, M. J. Lercel, B. M. La Fontaine, D. W. Myers, D. J. Brown, A. I. Ershov, R. L. Sandstrom, A. N. Bykanov, G. O. Vaschenko, N. R. Böwering, P. Das, V. B. Fleurov, K. Zhang, S. N. Srivastava, I. Ahmad, C. Rajyaguru, S. De Dea, W. J. Dunstan, P. Baumgart, T. Ishihara, R. D. Simmons, R. N. Jacques, R. A. Bergstedt, P. I. Porshnev, C. J. Wittak, M. R. Woolston, R. J. Rafac, J. Grava, A. A. Schafgans, Y. Tao, Proc. SPIE **8322**, 83221I (2012).
- [7] I. V. Fomenkov, N. R. Böwering, D. C. Brandt, D. J. Brown, A. N. Bykanov, A. I. Ershov, B. La Fontaine, M. J. Lercel, D. W. Myers, Proc. SPIE **8322**, 83222N (2012).
- [8] I. V. Fomenkov, B. La Fontaine, D. J. Brown, I. Ahmad, P. Baumgart, N. R. Böwering, D. C. Brandt, A. N. Bykanov, S. De Dea, N. R. Farrar, D. J. Golich, M. J. Lercel, D. W. Myers, C. Rajyaguru, S. N. Srivastava, Y. Tao, G. O. Vaschenko, Journal of Micro/Nanolith. MEMS MOEMS 11(2), 021110 (2012).

Lithography imaging control by enhanced monitoring of light source performance

Paolo Alagna^{*ab}, Omar Zurita^b, Ivan Lalovic^b, Nakgeun Seong^b, Gregory Rechtsteiner^b, Joshua Thornes^b

Koen D'have^c, Lieve Van Look^c, Joost Bekaert^c,

a) Cymer Inc., 17075 Thornmint Court, San Diego, CA 92127

b) Cymer Inc., Kapeldreef 75, 3001 Leuven, Belgium

c) IMEC, Kapeldreef 75, B-3001 Leuven, Belgium

ABSTRACT:

Reducing lithography pattern variability has become a critical enabler of ArF immersion scaling and is required to ensure consistent lithography process yield for sub-30nm device technologies. As DUV multi-patterning requirements continue to shrink, it is imperative that all sources of lithography variability are controlled throughout the product life-cycle, from technology development to high volume manufacturing. Recent developments of new ArF light-source metrology and monitoring capabilities have been introduced in order to improve lithography patterning control.^[1] These technologies enable performance monitoring of new light-source properties, relating to illumination stability, and enable new reporting and analysis of in-line performance.

In this paper, we discuss wafer patterning sensitivity to changes of the spatial and polarization properties of the light-source, which can now be monitored during wafer exposure. Wafer exposures have been carried out for line-space and contact-hole patterns using conventional and freeform illumination over a set of experimentally de-tuned light-source settings. Although the specific experiment conditions represent only a small sampling of the possible light-source operating space, the results show that changes in laser beam properties can have significant wafer patterning and illumination impacts for both 1D and 2D patterning. For line-space structures, for pitches from 88nm (CD 42nm) the changes measured with respect to the nominal conditions become significant, as well as the response of contact hole patterning resolved in a negative tone development process, where has been measured a shift of focus and done to size, induced by large polarization and divergence changes.

Therefore careful consideration is needed to determine the process-specific requirements for light-source performance, which can be determined using new beam metrology and monitoring enhancements. The new light-source metrology is applied to enhance light-source control over the lifetime of components and system service events, and is integrated within a comprehensive process monitoring and fault-detection methodology required for sub-30nm process technologies. This capability is in use by several chipmakers in order to reduce lithography patterning variability for sub-30nm device production.

1. INTRODUCTION:

The capability to control key contributors to lithographic process performance and productivity become extremely critical for leading edge lithography processes. It is therefore important to thoroughly characterize all sources of variation to determine opportunities for enhanced patterning control and increased productivity. Recent adoption of SMO (Source Mask Optimization)^{[2][3]} and freeform scanner illumination^{[2][3]} address the need for optimized patterning performance in ArF immersion lithography. Stable illumination and pupil performance is required in order to minimize patterning variations. Additionally, wide-spread use of double and multiple-patterning for sub-30nm technology also drives the need for high litho-cell productivity, requiring minimal down-time associated with light-source maintenance and return to full productivity following all service interventions.

1.2 Laser Parameter Monitoring

If we refer to the conventional lithography exposure tool and process metrics, it is well understood which parameters have critical influence on yield and productivity; looking in particular at the light source, the performance of bandwidth, wavelength and energy performance have been significantly improved over the several generations of ArF immersion light sources^{[4][5][6]}. The impact of bandwidth and wavelength variation and process performance was previously reported in literature^{[7][8][9]}.

Last year, Cymer introduced the capability to significantly enhance the light source control using a new on-board beam metrology system. This expands the existing metrology on the XL platform to provide real-time beam parameter measurements including far field (pointing and divergence), near field (energy density) and polarization components^[1].

Parameters	Impact
E95 bandwidth	Contrast, CD control
E95 bandwidth target	
FWHM bandwidth	
Energy average	Dose control
Energy sigma	
Wavelength sigma	Overlay, focus
Wavelength target	
Time stamp	Event correlation
Beam pointing	Illumination stability, contrast, system matching, troubleshooting (scanner vs. laser)
Beam divergence	
Beam size	
Beam energy density	
Polarization	Data integrity
Metrology integrity configurables	
Module pulse counts	
	Maintenance flagging

Table 1. Present and new XL laser platform metrology capabilities

The advanced on-board metrology is integrated with enhanced software data analysis system, which provides statistical analysis of performance sampled on a wafer basis. This product (SmartPulse™) enables chipmakers to monitor and correlate laser performance with each wafer exposed and therefore reduce lithography patterning variability. Additionally, the qualitative and quantitative information of 2D images of the light source beam generated by the system enables tool fingerprinting, and reduction of service and litho-cell requalification time. Work presented in collaboration with SAMSUNG^[1] at SPIE '12 shows how the on-board beam metrology can capture beam alignment changes after a service intervention and how those changes affect scanner pupil performance.

2. LITHOGRAPHIC IMPACT OF BEAM DIVERGENCE, POINTING AND POLARIZATION CHANGES

2.1 Experiment conditions

Wafer experiments of the lithography patterning impacts were performed at IMEC on the XLR 560i / XT 1900i lithography cluster. Changes in light source beam divergence, pointing and polarization were introduced using controlled advanced experimental techniques and were measured using the on-board metrology system installed on the light source. These parameters are described in Figure 1. Three different service scenarios were reproduced by varying the beam alignment conditions:

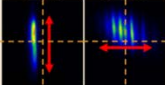
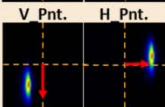
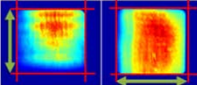
PARAMETER		IMAGE	DEFINITION
Divergence	Horizontal	Fair field 	Growth of the Horizontal dimension while it is propagating
	Vertical		Growth of the Vertical dimension while it is propagating
Pointing	Horizontal		Horizontal angle of laser beam while it is propagating
	Vertical		Vertical angle of laser beam while it is propagating
Beam size	Horizontal	Near field 	Horizontal dimension of beam
	Vertical		Vertical dimension of beam

Figure 1. Far field and near field parameters description.

Condition_1 : Divergence and Pointing change (module misalignment)

Condition_2 : Larger Divergence and Pointing change with respect to Condition_1 (module replacement)

Condition_3 : Polarization variation (degradation of laser optical part)

The achieved changes in laser beam parameter performance compared are shown in Table 2, in terms of differences from the nominal or baseline performance. The on-board metrology outputs were also used to recover the nominal system performance and is shown in the Return to Baseline.

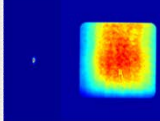
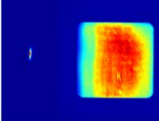
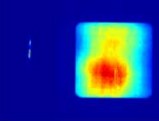
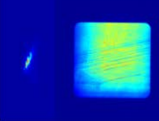
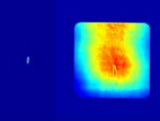
Deviation from BASELINE	BASELINE	CONDITION_1	CONDITION_2	CONDITION_3	RETURN TO BASELINE
Divergence (mRad)	0.0	0.8	1.4	1.3	0.2
Pointing (mRad)	0.0	1.2	1.3	0.1	0.1
Polarization (%)	0	0	0	-10	0
Metrology Camera Images					
NOTE	No changes on Wavelength and Bandwidth performances from Reference conditions.				

Table 2. Controlled beam experiment conditions

It is also important to emphasize that during the wafer experiments the optical performance of the light source in terms of bandwidth, wavelength and energy were not changed with respect to the baseline condition.

We tested performance of one parametric annular illumination condition (NA 1.35 / σ 0.94-0.79) and two freeform illuminations, targeting 41nm to 45 nm nominal CD for line-space and 70nm contact-hole patterns at different pitches. Hitachi CG-5000 CDSEM was used to measure the contact-holes, and ASML YS-200 scatterometry system was used for line-spaces to increase the measurement precision due to significant across-wafer sampling.

2.2 Scanner response

We measured wafer-plane intensity for each experiment condition, and observed a significant impact on the measured loss related to changes in pointing, divergence and polarization changes, with largest reduction in the case of Condition 3 (controlled use of degraded optical parts on the light source). The primary consequence of such variation is a potential throughput loss for high-dose applications. We estimated the reduction in scanner throughput, using the 83-field layout (with 26mm x 33mm field size) as a function of dose. At a dose-to-size of 40mJ/cm², we estimate that the throughput loss induced across our experimental conditions ranges between 5 to 15 wafers per hour (Wph), increasing even more for higher dose layers.

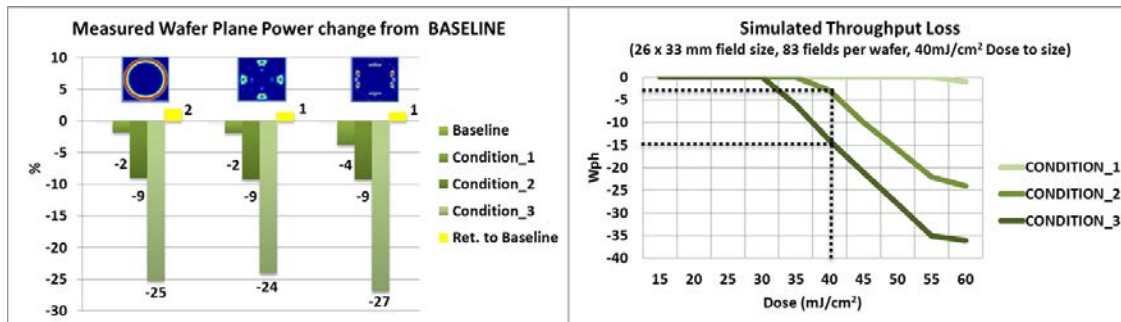


Figure 2. Wafer plane power change from the Baseline and the Simulated throughput loss per each condition.

Illumination pupil measurements obtained by the scanner (at the center of the slit) have been used to calculate the effective changes from the baseline comparing differences from each experiment condition to the baseline value. This provided qualitative and measurable pupil response information, for each of the measured illumination conditions.

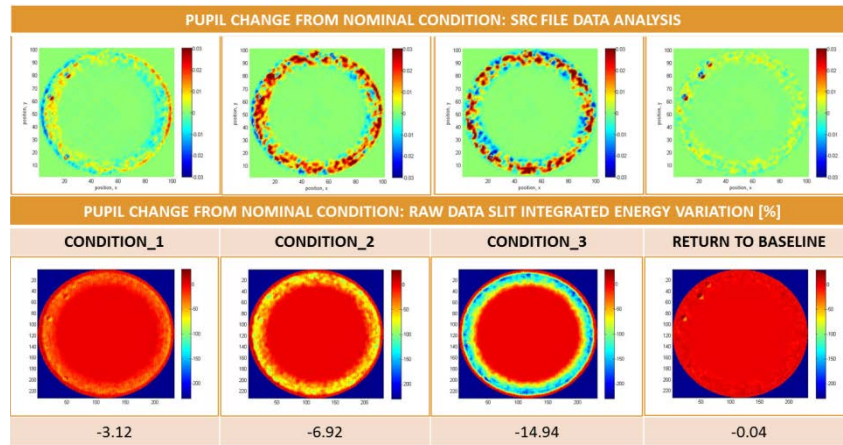


Figure 3. Comparison between conventional and raw data pupil analysis.

The analysis indicates interesting differences between responses of the different illumination conditions measured. We observe a direct correlation between the reduction of the wafer-plane power in Figure 2 and the annular integrated pupil- energy variation shown in Figure 3.

We also estimated with a high precision, the difference between the baseline starting point condition and the return to baseline following experiment conclusion, proving that it is possible to return to the original pupil image with an error of -0.04% on annular condition, which is largely within the test reproducibility measured over one month of operation.

2.3 Contact-hole Patterning Response

Analysis of the response of contact-hole patterning at the different beam conditions considered in this experiment was performed on a negative tone development (NTD) process. The process used is the same one optimized by IMEC for the experimental study of source mask optimization for 22nm SRAM cells^[3]

PARAMETER	UNIT	FREEFORM 2
NA		1.35
σ		0.865 – 0.654
Polarization		XY
TARGET	nm	70
	FEATU RE	CONTACT
PROCESS		NTD
FEM DOSE RANGE	mJ/c m ²	5 (0.5 steps)
FEM FOCUS RANGE	μm	0.4 (0.01 steps)
RESIST		FAiRS9521_M190 (NTD) [Fujifilm]

Table 3. Contact hole exposure conditions.

Six different contact-hole patterns in the SRAM layout, shown in Figure 4, were measured on wafers exposed across variation in focus and dose. The focus exposure matrix center dose was $25\text{mJ}/\text{cm}^2$ (with total range across wafer of $5\text{mJ}/\text{cm}^2$ with $0.5\text{mJ}/\text{cm}^2$ steps) and with center focus at $-0.1\mu\text{m}$ (with total range across wafer of $0.4\mu\text{m}$ with focus $0.01\mu\text{m}$ steps) as summarized in Figure 3 above.

The contact-hole pattern impacts from laser perturbation are significant. Condition_3 (Polarization and divergence variation from use of degraded laser optical parts) shows largest imaging impact. In this case, we observe a CD change common for all patterns targets, of approximately $+5\text{nm}$, which considering patterning using negative tone development process, is equivalent to a dose reduction and focus negative focus shift. A detailed analysis of the process windows using KLA-Tencor's ProData enables quantifying the effective change of the process window; the effective focus and dose shifts for Condition_3 compared to the Baseline setting correspond to approximately -20nm and $-1\text{mJ}/\text{cm}^2$ respectively.

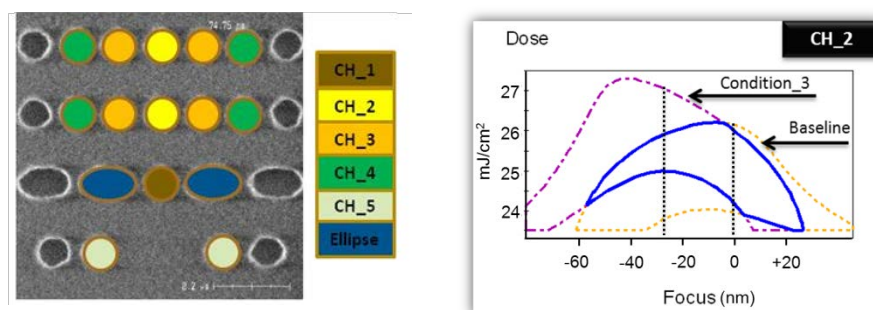


Figure 4. Contact hole measurement target and process windows comparison.

Process window analysis was used to show the impact on exposure latitude and depth of focus, confirming that this effect across the laser conditions achieved, and shows that the effect is consistent across the six patterns measured in the 22nm SRAM layout. The impact is largest for Condition_3, where the DOF is reduced by as much as 50%.

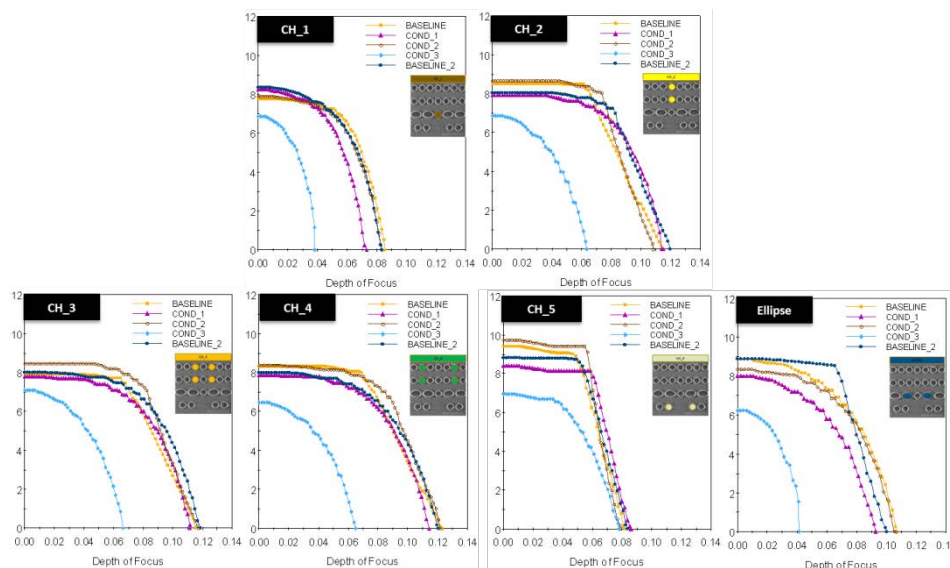


Figure 5. Exposure Latitude: response of diverse contact hole pitches to different light source experiment conditions.

2.4 CD Through Pitch response

The exposure conditions for 1D line-space structure patterning in our study are shown in Table 4.

PARAMETER	UNIT	ANNULAR	FREEFORM_1
NA		1.35	1.32
σ		0.94 – 0.79	
Polarization		XY	XY
TARGET	nm	41	
	nm	45	
	FEATURE	DENSE / ISO	DENSE / ISO
PROCESS		PTD	PTD
FEM DOSE RANGE	mJ/cm ²	10 (0.5 steps)	
FEM FOCUS RANGE	μm	0.240 (0.01 steps)	
RESIST		TARF-Pi6001ME [TOK]	

Table 4. Line-space exposure conditions.

The exposures were performed using a 1.35 NA, Annular, σ 0.94-0.74 XY Polarized, and a Freeform illumination at 1.35NA, with target critical dimensions between 42nm and 46nm through pitch, for pitches ranging from 88nm to 400nm, measured for both vertical and horizontal orientations

CD changes (average of horizontal and vertical features) from Baseline laser condition, have been analyzed for each experimental condition. Results show a CD increase as the pitch increases from dense (88nm pitch) to most contrast sensitive isolated patterns (400nm pitch). Care was taken to determine best focus at each condition independently for the line-space measurements; unlike the contact process window measurements, no changes in best focus are observed for line-space patterning.

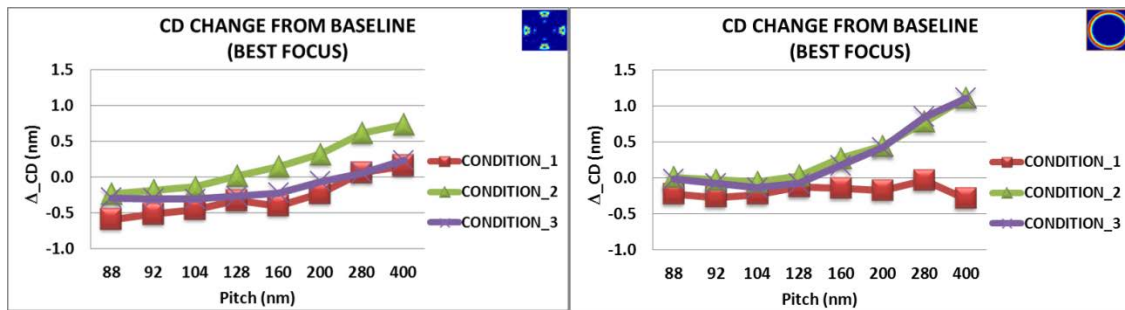


Figure 6. Through pitch CD change from nominal condition (measured at best focus)

Giving a closer look to the CD through focus change relative to the Baseline condition for two pitches (88nm and 200nm) shown in the next figure, it is possible to get a more accurate insight into the patterning response. In particular we notice that for dense pitches it is possible to have CD differences from the baseline of 0.25nm to 0.30nm which is approximately 0.7% of the nominal CD (42nm for this pitch) while for contrast sensitive pattern can reach up to 4% or 2nm (45nm of nominal CD at 200nm pitch).

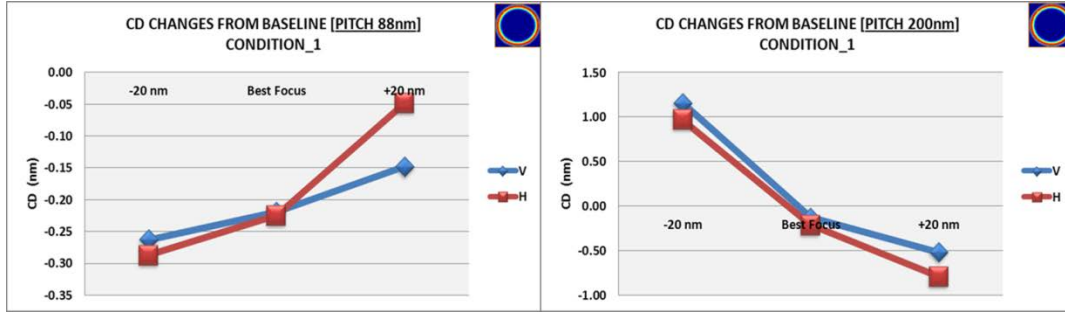


Figure 7. Pitch 88nm and 200nm through focus CD change from nominal condition.

This analysis has been applied to all the pitches for both illumination conditions, showing maximum impact on pitch 400 where the maximum measured Δ_{CD} (through focus) is approximately 10% (~4nm) from the nominal target at the Baseline condition.

2.5 CDU results

The CD uniformity across wafers for the most contrast sensitive pattern (Pitch 400nm) was also measured for constant focus and dose wafers exposures with annular illumination; we compared the Baseline wafer performance from that of Condition_3 over 83 full fields as well as wafers exposed at the completion of the experiments to obtain differences from the Return to Baseline. Using the proven metrology capability of the ASML YS-200 Scatterometry tool installed in IMEC facilities, we performed up to 104 intra-field measurements on the pitch 400nm target, collecting 17k measurements per wafer, and analyzed three sets of data :

1. Raw data average and 3σ
2. Intrafield average and 3σ
3. Corrected data (3σ) : Residual data after the removal of the intra-field average.

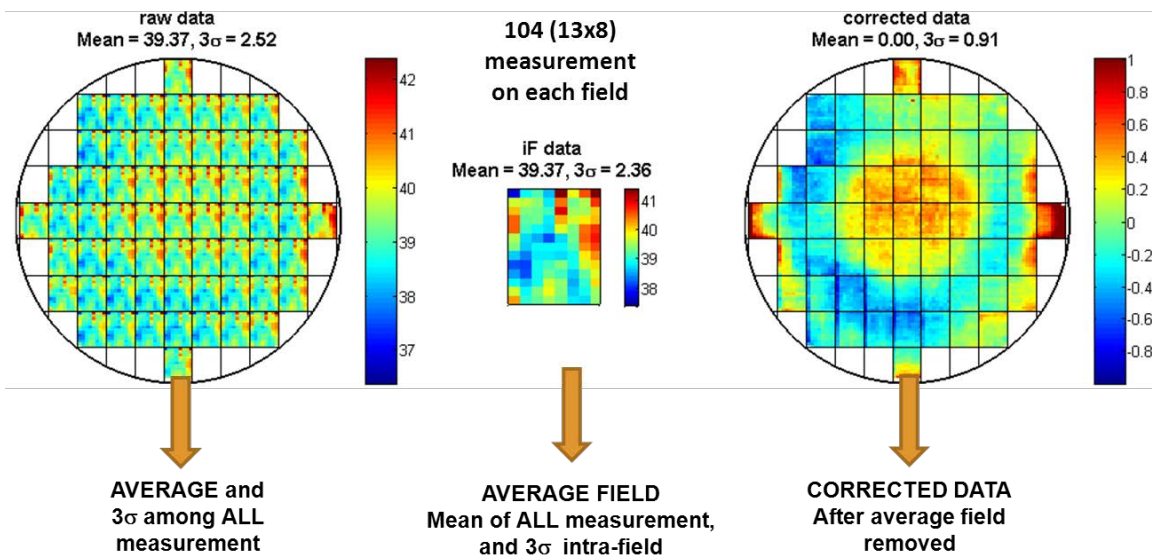


Figure 8. YS-200 measurement used for the across wafer and intra-field analysis.

The average across-wafer CD shows that difference between Condition_3 and Baseline is approximately 0.5nm, as shown in Figure 9 below. Removing the intra-field fingerprint (Corrected Data), the across-wafer CD uniformity difference between the two conditions (Condition_3 and Baseline) shows an impact of up to 0.7nm. Starting from the assumption that the process factors (track, reticle and scanner / process fingerprint) are constant between these wafer exposures, we expect that the most significant impact of the changes is related to the achieved differences in light-source condition. Furthermore, we see that both the differences in across-wafer CD average (for raw data) and the across wafer CD uniformity (corrected data) return to the nominal performance level following light-source Return to Baseline; the precision of the return condition is within the measurement reproducibility.

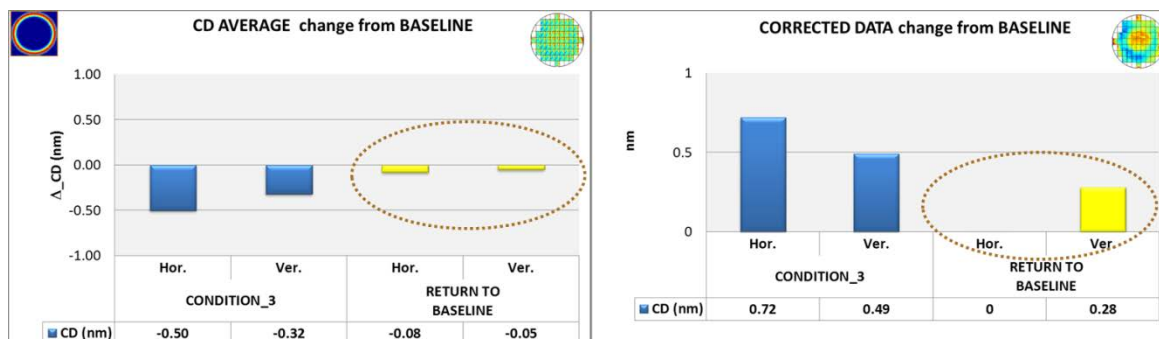


Figure 9. Changes from the Baseline: Condition_3 (Polarization and Divergence) and Return to Baseline.

3. INSTALL BASE DATA MONITORING

As discussed in the introduction, the stringent process control requirements that SMO and multiple patterning lithography require, it is becoming critical to improve the monitoring and variability control of lithography light-sources. Cymer has recently introduced the SmartPulse™ data product, which provides data associated with each exposed wafer and includes a range of optical (bandwidth, wavelength, energy) and beam propagation (divergence, pointing, size, polarization) parameters from the new on-board metrology. This is a significant enhancement over previous time-based data-sampling approaches, since it filters non-wafer exposure operation of the light-source, which adversely impacts the ability to correlate light-source performance with wafer patterning.

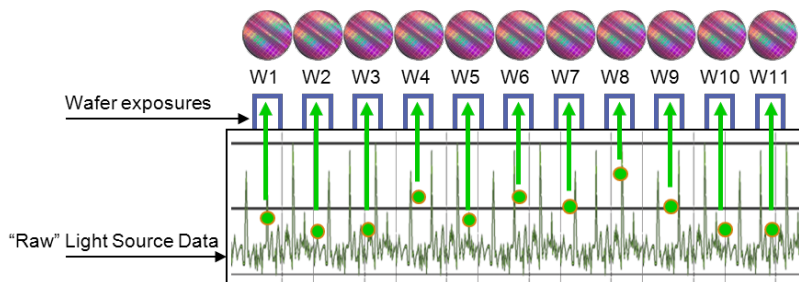


Figure 10. Smart Pulse™ : Laser metrology data associated to each wafer

SmartPulse™ product has already been adopted by chipmakers and is used in several production fabs. As shown in Figure 11, the user interface enables the end-user to manage light-source parameter performance and configurations in real-time and enables basic SPC alarming capability. The system can also be integrated with the factory automation systems for Fault Detection / Classification (FDC) or Statistical Process Control (SPC).

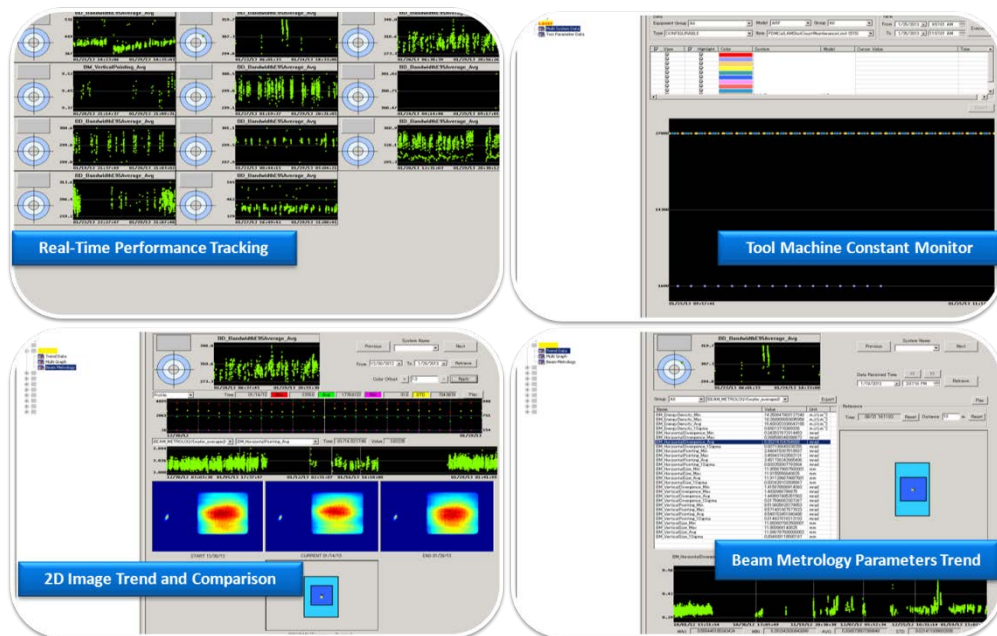


Figure 11. Smart Pulse TM : Graphic User Interface snapshots

The analysis shown in Figure 12, shows performance comparison of SmartPulseTM data from a chipmaker factory collected from nine different ArF systems including dry and immersion equipment for key beam parameters discussed in this paper. This enables comparison of laser performance across systems to quantify the variability between systems and over time, or over service events.

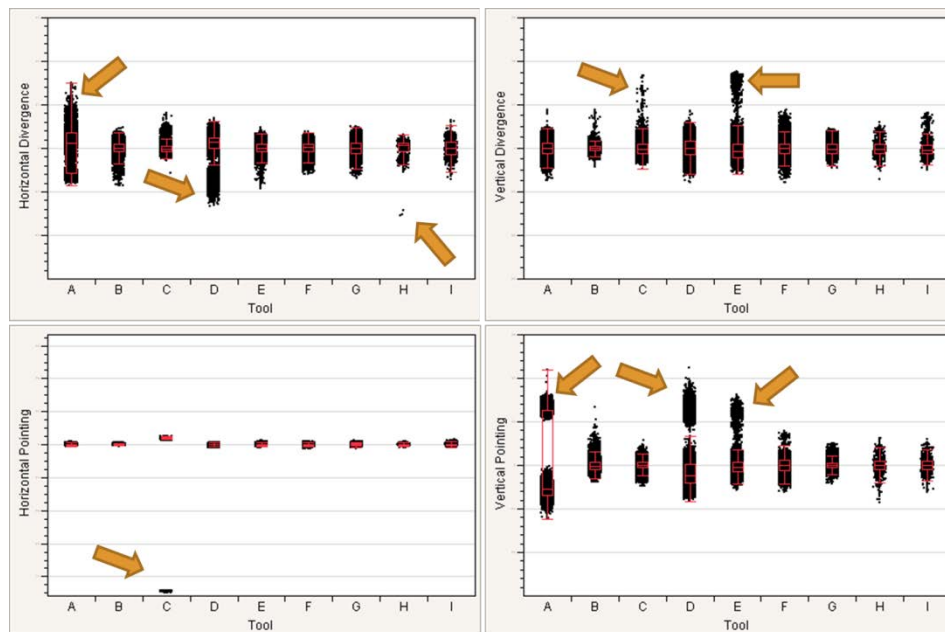


Figure 12. Smart PulseTM: Analysis of tool performance trends over 3months of operation in chipmaker fab

CONCLUSIONS

An experimental validation was carried out to estimate the lithographic effect (analyzed in a limited subset of illumination conditions) that different magnitudes of changes in light source beam divergence, pointing and polarization induce. To do so, the new on-board metrology unit developed by CYMER has been used to measure the applied controlled changes on the mentioned light source parameters. It was shown significant influence of polarization changes on 70nm SRAM contact hole defined in a negative tone development process, with a drift in CD of approximately 5 nm, induced by a focus shift of 20nm and dose to size change of -1mJ/cm². Critical effect was measured also in the patterning of line-space, where for contrast-sensitive patterns changes is in the range of 2nm to 4nm (<10%) of nominal CD, with <1% dense line-space CD impact. The studied cases were also correlated to a measurement of wafer-plane power reduction up to 30%, which would lead to productivity loss for high-dose applications. The advantage of the new metrology capability was also demonstrated restoring the original beam characteristics, with an error which is in the range of the metrology system measurement reproducibility. Finally it has been demonstrated how SMART PULSETM data product, which integrates new on-board laser metrology, is used by chipmakers to monitor and analyze on-wafer performance of installed light-sources, and drive improvements in CD control.

ACKNOWLEDGEMENTS

The authors are very grateful for all support given to this project. In particular, Jason Lee, James Bonafede, Simon Hsieh, Yoo Keun Won, Remo Petrella, Thomas Giese, Gerald Lichtenberg, Emile Merkus, Tommy Oga, GG Padmabandu, Slava Rokitski, Nigel Farrar (CYMER), Anne-Laure Charley, Jeroen Van de Kerkhove, David Laidler, Wouter Pypen (IMEC), Fuchimoto Daisuke, Sakai Kei (Hitachi) are acknowledged for their help, practical discussions and organizational support.

REFERENCES:

- [1] J. Choi et al., "Enhancing lithography process control through advanced, on-board beam parameter metrology for wafer level monitoring of light source parameters," Proc. SPIE Optical Microlithography XXV 8236,99 (2012).
- [2] K. Iwase et al. "A new source optimization approach for 2X node logic", Proc. SPIE. 8166 Photomask Technology 2011
- [3] J. Bekaert et al. "Freeform illumination sources : an experimental study of source-mask optimization for 22-nm SRAM cells" Proc. SPIE 7640, Optical Microlithography XXIII, 7640,08 (2010);
- [4] T. Cacouris et al. "Advanced light source technologies that enable high-volume manufacturing of DUV lithography extensions" SPIE Proc. Vol. 8326 (2012)
- [5] R. Rokitski et al. "High reliability ArF light source for double patterning immersion lithography", Proc. SPIE Vol. 7640 (2010)
- [6] R. Rokitski et al. "High-power 120W ArF immersion laser for high-dose applications", Proc. SPIE Vol. 8683 (2013)
- [7] I. Lalovic et al. "Fast and accurate laser bandwidth modeling of optical proximity effects", Proc. SPIE 6730, Photomask Technology 2007, 67301X
- [8] N. Seong, et al. "Analysis of the effect of laser bandwidth on imaging of memory patterns", Proc. SPIE 7140, Lithography Asia 2008, 714042
- [9] U. Iessi et al. "Laser bandwidth effect on overlay budget and imaging for the 45 nm and 32nm technology nodes with immersion lithography", Proc. SPIE 7973, Optical Microlithography XXIV, 797328
- [10] J. Bekaert et al., "60nm half pitch contact layer printing: exploring the limits at 1.35NA lithography", Proc. SPIE Optical Microlithography XXI, 6924,3A (2008)